Applied Thermal Engineering 254 (2024) 123724

Contents lists available at ScienceDirect

Applied Thermal Engineering

journal homepage: www.elsevier.com/locate/ate

Research Paper

A novel methodology for map-based model fitting: A case study with a Dual Source Heat Pump experimental dataset

Javier Marchante-Avellaneda [a,*], Emilio Navarro-Peris [a], Francisco Barceló-Ruescas [a], Yang Song [b]

[a] Instituto Universitario de Investigación en Ingeniería Energética, Universitat Politècnica de València, Camino de Vera s/n, 46022 Valencia, Spain
[b] Department of Energy Technology, Division of Applied Thermodynamics and Refrigeration, Royal Institute of Technology, SE-100 44, Stockholm, Sweden

ARTICLE INFO

Keywords:
Empirical models
Heat pump performance
Dual Source Heat Pump
Design of Experiments
New fitting approach

ABSTRACT

This paper presents a new methodology to adjust map-based models to experimental data and reports the main results of a comprehensive experimental campaign of a Dual Source Heat Pump (DSHP) prototype. The prototype tested incorporates variable speed components (compressor, circulation pumps, and fan). The novelty of this prototype lies in its ability to select two possible heat sources: air or ground. Thus, it can operate as a geothermal or aerothermal heat pump, as well as a chiller, thanks to the additional capacity to reverse the cycle. Thanks to this hybrid approach, several advantages can be obtained compared to conventional equipment, such as higher efficiency, the requirement of smaller borehole heat exchangers, or the absence of defrost cycles. In a prior study, polynomial models were developed to accurately characterize the DSHP's performance (*i.e.*, condenser and evaporator capacities and electrical energy consumption). These models were obtained considering the external variables to the unit as independent variables to facilitate their applicability using variables commonly measured in real installations. Due to the complexity of heat pump performance, which in current equipment can be influenced by up to 5 or 6 independent variables, the search for suitable polynomial models required the availability of a complete working map including more than 3000 working points. Thus, this previous work developed these models based only on simulation results. In this sense, this paper concludes the development of these models by focusing on two critical issues concerning empirical model development. The first aspect involves determining the minimum number and location of testing points needed to define the experimental sample for the model adjustment. The reported experimental data were obtained by analyzing the most suitable experimental design methodology to create the experimental matrices in each operating mode of the DSHP. The second aspect focuses on the final adjustment of models using experimental data. A novel fitting approach for empirical models is introduced in the last part of this study. The developed methodology enables the integration of simulation and experimental results for the final fitting of empirical models through a two-step adjustment. The first step involves analyzing and defining polynomial functionals from the complete working maps generated by simulation. Subsequently, in a second step, the polynomial models are refitted to a suitable experimental sample using the methodology presented in this work. The latter allows for the increase of the accuracy of the models and the minimization of experimental costs. This novel approach ensures a robust characterization of systems with many independent variables using a minimum amount of experimental data. Significant benefits can be obtained from its application, such as the reduction of experimental cost and an increase in the model's accuracy through an effective combination of both experimental and simulated information. Furthermore, it can be considered of general applicability to other engineering problems where the characterization of physical systems influenced by a high number of independent variables is required.

1. Introduction

Heat Pump (HP) technology plays a crucial role in modern heating and air-conditioning applications for buildings, offering a sustainable and energy-efficient alternative to conventional fossil fuel boiler systems [1,2]. The significance of this technology is underscored by the European Union's commitment to renewable energy sources, as evidenced by the current REpower plan [3]. This plan emphasizes the

* Corresponding author.
E-mail addresses: jamarav@iie.upv.es (J. Marchante-Avellaneda), emilio.navarro@iie.upv.es (E. Navarro-Peris), fbarcelo@iie.upv.es (F. Barceló-Ruescas), yson@kth.se (Y. Song).

https://doi.org/10.1016/j.applthermaleng.2024.123724
Received 29 January 2024; Received in revised form 15 May 2024; Accepted 16 June 2024
Available online 21 June 2024

Nomenclature

Acronyms

ASHP	Air Source Heat Pump
BPHE	Braze Plate Heat Exchanger
CCD	Central Composite Design
CV_{RMSE}	Coefficient of Variation of the RMSE
DHWA	Domestic Hot Water Air operating mode
DHWG	Domestic Hot Water Ground operating mode
DHWU	Domestic Hot Water User operating mode
DoE	Design of Experiments
DSHP	Dual Source Heat Pump
GSHP	Ground Source Heat Pump
HP	Heat Pump
HVAC	Heating, Ventilating, and Air-Conditioning
MRE	Maximum Relative Error (%)
PHE	Plate Heat Exchanger
PID	Proportional Integral Derivative controller
RMSE	Root Mean Square Error (W)
RSM	Response Surface Methodology
RTD	Resistance Temperature Detector
RTPFHx	Round Tube Plate Fin Heat exchanger
SA	Summer Air operating mode
SG	Summer Ground operating mode
WA	Winter Air operating mode
WG	Winter Ground operating mode

Symbols

dT_c	Temperature difference of the secondary fluid across the condenser (K)
dT_e	Temperature difference of the secondary fluid across the evaporator (K)
f_c	Compressor frequency (Hz)
f_{fan}	Fan speed (%)
$P_{h,user}$	Circulation pump hydraulic power, user loop (W)
$P_{h,ground}$	Circulation pump hydraulic power, ground loop (W)
$\dot{Q}_c$	Condenser capacity (W)
$\dot{Q}_{cooling}$	Cooling capacity (W)
$\dot{Q}_e$	Evaporator capacity (W)
$\dot{Q}_{heating}$	Heating capacity (W)
RH	Relative humidity (%)
T_{ci}	Inlet temperature of the secondary fluid to the condenser (K)
T_{co}	Outlet temperature of the secondary fluid to the condenser (K)
T_{ei}	Inlet temperature of the secondary fluid to the evaporator (K)
T_{eo}	Outlet temperature of the secondary fluid to the evaporator (K)
$\dot{W}_c$	Compressor energy consumption (W)
$\dot{W}_{DSHP}$	DSHP energy consumption (W)
$\dot{W}_{par}$	Parasitic consumption (W)
$\dot{W}_{ground,pump}$	Circulation pump energy consumption, ground loop (W)
$\dot{W}_{user,pump}$	Circulation pump energy consumption, user loop (W)
w_{ai}	Humidity ratio at RTPFHx inlet conditions ($kg_{water}/kg_{dry\ air}$)
w_{sat}	Humidity ratio at saturated conditions ($kg_{water}/kg_{dry\ air}$)
Δw	$w_{ai} - w_{sat}$ ($kg_{water}/kg_{dry\ air}$)
$\Delta w'$	$\max[w_{ai} - w_{sat}, 0]$ ($kg_{water}/kg_{dry\ air}$)
η_p	Circulation pump motor efficiency (%)

importance of transitioning towards cleaner energy solutions to address climate change concerns. Additionally, the European Commission's upcoming HP action plan shows an increased emphasis on advancing HP technology. It aims to increase the number of installed HP units in Europe by 60 million more by 2030. This underscores the technology's pivotal role in contributing to the broader goals of energy sustainability and environmental responsibility within the European Union.

Concerning HP technologies, Ground Source Heat Pumps (GSHP) is one of the least carbon-intensive Heating, Ventilating, and Air-Conditioning (HVAC) technologies [4,5]. Furthermore, compared to the Air Source Heat Pump (ASHP), GSHP presents more stable source temperatures. This results in increased efficiency, with the only negative aspect being their installation cost. One potential strategy for installation cost-saving in GSHP involves integrating it with an additional thermal source through the use of hybrid systems [6,7]. In this sense, manufacturers have been refining system designs and introducing new concept units, such as hybrid systems like Dual Source Heat Pumps (DSHPs). These new units enhance system complexity if we compare DSHPs with conventional GSHPs. However, the availability of different heat sources enables a reduction in borehole heat exchanger size, thus decreasing the installation costs of these units.

DSHP technology implies the development of hybrid systems allowing these units to switch between different heat sources, such as using air or ground as the sources. This flexibility enhances overall performance by strategically selecting the optimal heat source based on boundary conditions like air and ground temperatures. It allows, for example, the elimination of possible defrost cycles common in ASHPs by simply selecting the ground as a source under frost conditions. However, developing effective control strategies relies heavily on accurately modeling and characterizing HP units. Therefore, accurately modeling these units is essential when setting an optimal control to determine the more convenient source type. This ensures optimizing such systems, which contributes to using more efficient units and assists in developing heat pump technology.

Regarding HP system characterization, the construction and adjustment of HP models is a common task faced up by researchers. In general, system characterization involves precisely defining a variable of interest, typically denoted as the response variable (y), using different modeling strategies. This variable y is influenced by a set of independent variables ($x_1, x_2, \ldots, x_n$), fixing them the boundary conditions. In some cases, the relationship between both is known exactly based on physical or chemical laws, resulting in a mechanistic or theoretical model like $y = g(x_1, x_2, \ldots, x_n)$. However, when the underlying mechanism is not fully understood, researchers must approximate the unknown function g with an empirical model: $y = f(x_1, x_2, \ldots, x_n)$, where polynomial models are commonly chosen as suitable functionals.

In the field of Heat Pumps, characterizing response variables involves building models to predict heat pump performance, *i.e.*, heating and cooling capacities as well as energy consumption. The literature contains some publications for both theoretical and empirical models. Some examples of HP models including a detailed description for each individual HP component are implemented in several simulation software like the ORNL Heat Pump Design Model [8], the CYCLE_D-HX [9]

or the IMST-ART [10] simulation software. On the other hand, despite being a less developed topic, several simple empirical models have been reported in the literature, such as the Hamilton [11], Tabatabaei [12], or Verhelst [13] models, where polynomial models are reported for the prediction of heat pump performance. However, these models have been reported for relatively simple units and with a limited number of control variables.

From both approaches, empirical models offer simple correlations. They serve as efficient black-box models with advantages like low computation time and improved accuracy, especially when adjusting them with numerous experimental tests [14]. This explains why this approach is the most widespread for modeling, for example, one of the main components installed in these units, the compressor [15].

As mentioned above, existing empirical models for HP units are underdeveloped, primarily covering very simple units. The introduction of variable speed components like compressors, circulation pumps and fans is a common practice in current designs. Including them, the manufacturers are able to obtain more flexible units that can adapt to the required user demand, such as varying the compressor speed when operating under partial load conditions. However, the introduction of these new components complicates empirical modeling due to the increased number of boundary variables. This implies that it is necessary to investigate how to perform an effective experimental characterization of current heat pump designs, where the installation of variable speed components has led to a considerable increase in the control variables of these systems.

In this sense, several polynomial models characterizing HP performance were presented in a previous study [16]. These models were developed by using the analyzed unit in this work, a reversible dual source heat pump including variable speed components, in order to obtain suitable empirical models for current HP and chillers designs and different technologies (aerothermal and geothermal units). This previous work developed these polynomial models as a function of the external variables and dealt with the huge number of independent variables by fitting the polynomial models with the complete working maps of the unit generated by simulation.

However, some aspects related to the experimental characterization of current HP designs that were not covered in this previous study still need to be clarified, such as:

- Can experimental data be used to improve the developed polynomial models?
- How can the information obtained by simulation be combined with the experimental results to obtain a better characterization of HP units?
- How many test points are necessary, and where should they be located on the working map to obtain a suitable experimental sample?

Against this background, this study aims to conclude the development of the models presented in [16] by addressing the abovementioned issues. The novelty of this study lies in developing a novel methodology to characterize current heat pump designs, including how to obtain suitable polynomial expressions and how to perform the experimental matrices to obtain the required experimental information.

To this end, an analysis has been carried out to identify possible experimental designs in order to define the number of tests and their location in the working map of the unit. Once the most suitable experimental design was identified, several experimental matrices were formed, and an extensive experimental campaign was carried out. The results of this experimental campaign are reported in this study (227 points in a total of 7 operating modes). Given the hybrid typology and ability to invert the cycle of this unit, the data reported are representative of the main heat pumps and chillers – aerothermal and geothermal units – present in the market. Finally, this paper also reports the final adjustment of the models by introducing a novel fitting methodology that combines simulated results with experimental data. The main objective will be to provide a well-defined methodology to assist the characterization of any type of system or process with many independent variables. It allows for a decrease in the experimental costs when dealing with such types of systems or processes while obtaining robust and accurate models that benefit from both experimental and simulated information.

2. Methodology

This section introduces the methodology used to improve the polynomial models developed in [16] using the experimental information collected in the laboratory for the analyzed DSHP. In order to assist the reader in understanding the contents of this work, we will refer to the polynomial models reported in [16] as *"base polynomial models"*, showing in a sequential and ordered way the methodology developed in the present work to obtain the *"corrected polynomial models"* using the reported experimental information. Furthermore, a brief description of the characterized unit is included below, listing the various operating modes of the unit and including a summary of the methodology developed that will be complemented with the following two sections. The complete process involves the initial model construction reported in [16], followed by a model readjustment using experimental results. This study focuses on constructing the experimental matrices through the Design of Experiment methodologies to obtain the required experimental information. Then, based on these experimental test matrices, the empirical results were generated in the laboratory. This work concludes by proposing a novel model refitting approach using the collected experimental data to improve the accuracy of the *"base polynomial models"* when predicting the unit performance.

2.1. DSHP unit

This DSHP is the first of three prototypes developed and designed inside the framework of the GEOTeCH project [17]. It is a unit with variable speed components (compressor, fan, and circulation pumps), R32 as refrigerant fluid, 8 kW of nominal heating capacity, a total of three Braze Plate Heat Exchangers (BPHE), and a Round Tube Plate Fin Heat exchanger (RTPFHx). This unit is designed to work at a constant superheat value of 5 K and a SC $\approx$ 0 K (it includes a liquid receiver installed at the condenser outlet). All these components are included to allow the unit to operate as a ground or air source system and provide the user with cooling, heating, and Domestic Hot Water (DHW) production. A simple layout of the unit is provided in Fig. 1, exemplifying the interconnection of elements in two of the seven possible operating modes. The green lines show how the refrigerant flows through the several elements of the DSHP depending on the operating mode selected by opening different solenoid valves. The red lines include those lines sectioned by closed solenoid valves or check valves. More details concerning the DSHP unit and its components can be found in [16,18].

As can be seen in Fig. 1, the unit is provided with a suitable interconnection of solenoid valves and check valves. Valves SA1, SD, SG1, and SU1 are used to select the heat exchanger to be used as the condenser. Then, SA2/SAS, SG2/SGS, and SU2/SUS valves are used to select the evaporator, and the check valves are positioned so that the flow through the expansion valve always maintains the same direction. According to this arrangement, the unit can operate in 7 operating modes. Table 1 shows these 7 operating modes and the nomenclature used in this work to refer to them.

The operating modes are categorized into heating (winter) and cooling (summer). Winter modes – denoted as Winter Ground (WG) or Winter Air (WA) – involve selecting ground or air as the heat source when the unit operates as a heat pump. Corresponding modes for cooling are Summer Ground (SG) and Summer Air (SA), producing chilled water for the user. DHW Ground (DHWG) and DHW Air (DHWA) are

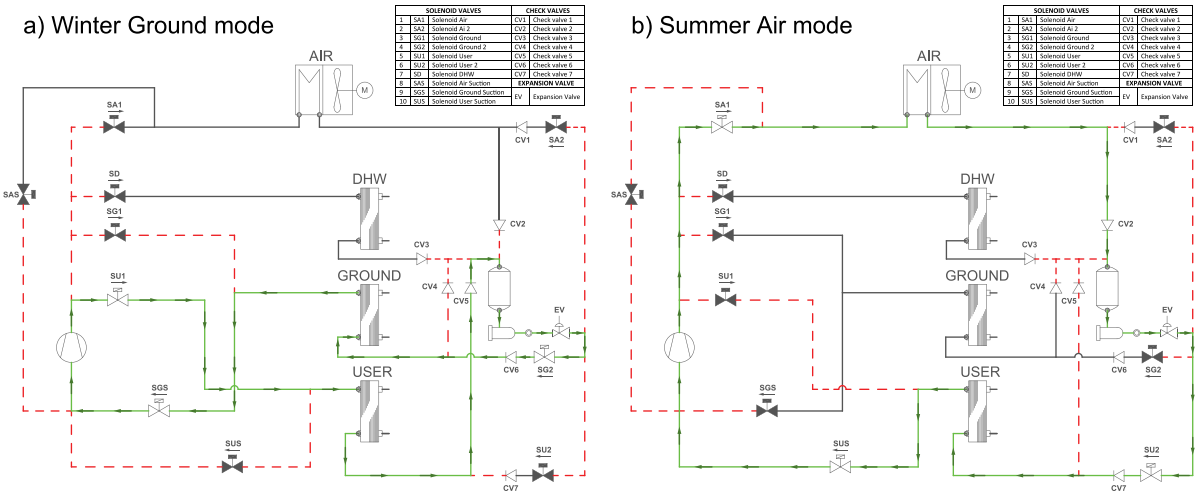

Fig. 1. DSHP: Winter Ground and Summer Air modes schemes.

Table 1
Operating modes.

Mode	Summer		Mode	Winter	
	Condenser	Evaporator		Condenser	Evaporator
Heating & Cooling					
1-SA[a]	Air	User	4-WA[f]	User	Air
2-SG[b]	Ground	User	5-WG[g]	User	Ground
DHW & Cooling					
3-DHWU[c]	DHW	User			
Domestic Hot Water					
6S-DHWA[d]	DHW	Air	6W-DHWA[d]	DHW	Air
7S-DHWG[e]	DHW	Ground	7W-DHWG[e]	DHW	Ground

[a] SA: Summer Air.
[b] SG: Summer Ground.
[c] DHWU: Domestic Hot Water User.
[d] DHWA: Domestic Hot Water Air.
[e] DHWG: Domestic Hot Water Ground.
[f] WA: Winter Air.
[g] WG: Winter Ground.

domestic hot water production modes in winter and summer conditions, and the polynomial models for these modes are constructed to predict unit performance in both seasons. Finally, the additional DHW User (DHWU) mode is intended to operate in cooling mode while there is a demand for domestic hot water production in summer.

2.2. Empirical model development approach

The *"base polynomial models"* reported in [16] include three polynomial models per mode to predict the DSHP performance as a function of 5 to 6 independent variables. These variables include inlet/outlet temperatures of water supplied to the user, inlet/outlet temperatures of brine, inlet air temperature and humidity, and compressor and fan frequency, depending on the operating mode (More details related to the independent variables selection can be found in [16]). In this previous work, the approach selected was to eliminate the effect of the auxiliaries components to facilitate the development of these models, *i.e.*, the effect of the internal circulation pumps, fan, and electrical parasitic consumption. Thus, selecting Winter Ground mode as an example, Eqs. (1), (2), (3) show how the effect of the circulation pumps and the parasitic consumption of the unit should be included:

Winter Ground — Performance including the auxiliary components

$$\dot{Q}_{heating} = \boxed{\dot{Q}_c(f_c, T_{eo}, dT_e, T_{co}, dT_c)} + \left[\eta_p \cdot \dot{W}_{user,pump} - P_{h,user}\right] \quad (1)$$

$$\dot{Q}_{cooling} = \boxed{\dot{Q}_e(f_c, T_{eo}, dT_e, T_{co}, dT_c)} - \left[\eta_p \cdot \dot{W}_{ground,pump} - P_{h,ground}\right] \quad (2)$$

$$\dot{W}_{DSHP} = \boxed{\dot{W}_c(f_c, T_{eo}, dT_e, T_{co}, dT_c)} + \dot{W}_{par} + \dot{W}_{user,pump} + \dot{W}_{ground,pump} \quad (3)$$

Although the effect of the auxiliaries only implies a slight correction of the unit performance, the characterization of the auxiliaries was included in the supplementary material of [16]. It can be consulted in order to consider their effect. The highlighted parts in the equations refer to the polynomial models developed for the prediction of the condenser and evaporator capacities ($\dot{Q}_c$ and $\dot{Q}_e$) as well as the compressor energy consumption ($\dot{W}_c$). Eq. (4) illustrates as an example the *"base polynomial model"* for the compressor energy consumption prediction in Winter Ground mode:

$$\dot{W}_c = f_c\,(a_0 + a_1 T_{co}^2 + a_2 T_{co} + a_3 T_{eo}^2 + a_4 T_{eo} + a_5 dT_c + a_6 dT_e + a_7 f_c + a_8 1/f_c + a_9 T_{co} T_{eo} + a_{10} T_{co} dT_c + a_{11} T_{eo} f_c) \quad (4)$$

Where f_c is the compressor speed, T_{ci} and T_{co} are the inlet and outlet temperatures of water in the condenser, and T_{ei} and T_{eo} are the inlet and outlet temperatures of brine in the evaporator.

Since the *"base polynomial models"* were solely based on simulation results, the present work aims to enhance the prediction power of these models by using experimental data in order to obtain more accurate models. The main objective is to define a more general methodology to develop empirical models by combining simulation and experimental results. It can be considered of general applicability to any other type of system and allows us to deal with the problem of characterizing systems with many control variables. The requirements for its applicability lie in the availability of a detailed model to generate the working maps through simulation and to dispose of a suitable test bench to carry out the experimental tests. In that way, we will obtain compact and easy-to-implement models that are more accurate because experimental data have refined them.

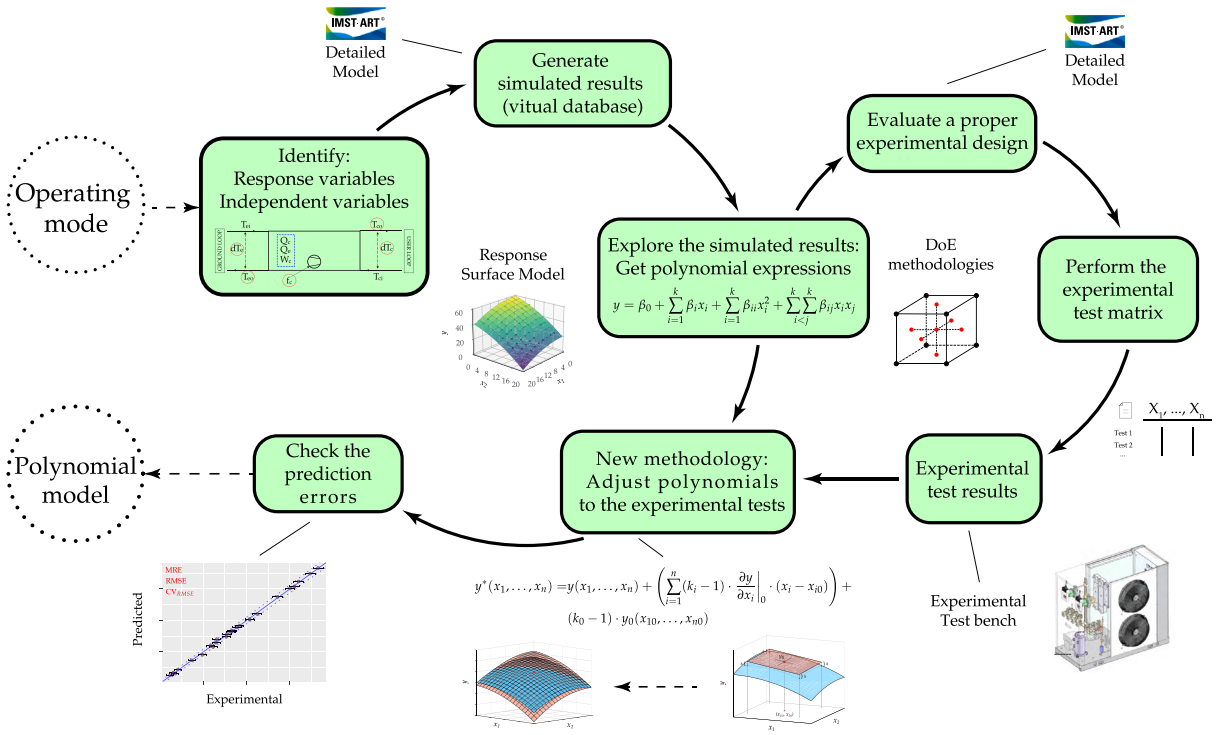

Fig. 2. Steps to obtain polynomial models using simulated and experimental information.

For the analyzed unit in this work, obtaining the final empirical models involves the following steps, also illustrated in Fig. 2:

1. Generation of the unit working maps in each operating mode. For this purpose, the detailed model of the DSHP in IMST-ART and reported in [16] has been used to obtain simulation data.
2. Study of the simulation data to compose suitable polynomial expressions in each operating mode.
3. Determination of the most appropriate experimental design to perform the experimental test matrices. The IMST-ART model is also used for this purpose.
4. Generate the experimental results on the test bench.
5. Adjustment of the polynomials to the experimental data. At this point, a novel methodology has been defined to combine the information extracted from the simulation and experimental data.

The first two steps were already carried out during the development of the *"base polynomial models"*. In this previous work, the working maps were obtained in the 7 operating modes by developing a virtual database with a total of 21875 points (3125 points by operating mode) using a detailed model of the unit in the IMST-ART software. As mentioned above, the most appropriate polynomial expressions were obtained to predict the condenser and evaporator capacities and the compressor energy consumption from the analysis of this data, where the regression coefficients were adjusted using the virtual database (*e.g.*, coefficients a_0 to a_{11} in Eq. (4) were adjusted with 3125 simulation points).

This paper will focus on the last three steps. In order to simplify the explanation of the contents to the reader, this work has been divided into the following sections:

- Section 3 includes an analysis in order to perform the required experimental matrices. This implies knowledge related to the number of points to be tested and where to place them on the working map of the unit. It includes the following contents:
  - Section 3.1: Comparison of suitable experimental designs for HP system characterization.
  - Section 3.2: Selection of the most appropriate experimental design to perform the required experimental matrices. The experimental matrices were constructed according to the selected experimental design, defining the number of test points and their location in the unit operating range.
  - Section 3.3: It introduces the experimental test rig used to conduct the DSHP experimental campaign.
  - Section 3.4: It summarizes the number of points tested in the laboratory, where a complete report for all the experimental measurements is included as supplementary material.
- Section 4 describes the novel fitting methodology developed, where the *"base polynomial models"* are refitted with the experimental information generated in this work.
- Section 5 summarizes the prediction errors by comparing the *"base polynomial models"* with the *"corrected polynomial models"* developed in this work.

The error metrics used in this work include: the Maximum Relative Error (MRE), the Root Mean Square Error (RMSE), and the Coefficient of Variation of the RMSE (CV_{RMSE}), *i.e.*, the ratio of the RMSE to the mean of the response variable. Regarding the means and software tools required to develop the present study, a suitable test bench has been used to collect the experimental information. The tool selected to conduct the regression adjustment was the R software [19] and the IDE RStudio [20]. The IMST-ART simulation software [21] and the detailed model of the unit reported in [16] were used to generate the required simulation results to conduct the DoE methodology comparison. Finally, the thermophysical properties were calculated with the software Engineering Equation Solver (EES) [22]. EES software was also used for the corresponding uncertainty analysis of the experimental data.

3. Experimental dataset

This section details the experimental campaign collected for the analyzed DSHP, outlining the strategy employed to construct the experimental test matrices. Comprising four subsections, the first and second one assesses several Designs of Experiment methodologies, comparing them and selecting the optimal experimental design for defining the size and test point location to obtain a suitable empirical sample in each operating mode. The subsequent subsection outlines the experimental test rig and sensors used to collect the experimental results. At the end of this section, a brief summary reports the experimental data collected from the seven operating modes of the analyzed DSHP. The experimental data – including measurement uncertainty – are included as supplementary material to this work.

3.1. Design of experiments methodologies selected

From the *"base polynomial models"*, the present work focuses on properly refitting these models using experimental data. So, experimental information must be generated, and a suitable approach to readjust the models is required. For the first purpose, the Design of Experiments (DoE) methodologies are a powerful tool that can be used to define a suitable sample of experimental points with the maximum statistical inference, providing an accurate description of how the unit works.

DoE is defined as a branch of statistics that deals with planning and conducting the experimental stage, and it is used together with the Response Surface Methodology (RSM) in order to construct empirical polynomial models.

Two main types of DoE exist: classical DoE, featuring well-documented experimental matrices from the available literature, and computer-aided design, which employs calculations assisted by computers and predefined algorithms. In order to simplify matrix construction without additional tools, this work opts for the classical DoE typology. Its ease of implementation enables planning in a simple way the experimental tests required to readjust the *"base polynomial models"*.

Concerning classical DoE methodologies, factorial design is one of the simplest and most widely used approaches. A complete factorial design with k independent variables involves selecting n_{x1} levels for x_1, n_{x2} levels for x_2, and so on, resulting in a total of $n = n_{x1} \times n_{x2} \times \cdots \times n_{xk}$ points. The orthogonality property of factorial designs is advantageous because it ensures that estimating the effect of one variable or interaction remains uninfluenced by others when constructing empirical models based on polynomial functions.

However, the main problem of this approach is the rapid increase in the number of tests when incorporating more variables or levels in the design. For instance, with five independent variables and five levels for each one, the total experimental points would reach $5^5 = 3125$.

To mitigate this challenge, the concepts of blocking and fractionating experimental designs [23, chap. 5] offer effective ways to reduce the overall number of experimental points. This can be illustrated with a simplified example depicted in Fig. 3, where a complete two-level factorial design (left-hand) is also divided into two blocks (right-hand). This example is provided to exemplify in a simple way to the reader several key concepts when planning an experimental design, ending with the selection of several experimental designs for the characterization of five independent variable systems (like the analyzed unit).

In the 2^3 design represented in Fig. 3 there are a total of 8 runs in which each independent variable occurs at just two levels (−1 and +1). The first possibility is to run the complete factorial design in a random order, testing all the points included in Table 2.

Table 2
Two blocks for a 2^3 design.

x_1	x_2	x_3	$x_1x_2x_3$	Block
−1	−1	−1	−1	I
+1	−1	−1	+1	II
−1	+1	−1	+1	II
+1	+1	−1	−1	I
−1	−1	+1	+1	II
+1	−1	+1	−1	I
−1	+1	+1	−1	I
+1	+1	+1	+1	II

However, a better approach may have been to run the experimental design in a series of randomized blocks. Suppose, for example, that we are characterizing the velocity at the inlet section of a Round Tube Plate Fin Heat exchanger (RTPFHx) and the independent variables in Table 2 are the fan speed, the temperature set in the climatic chamber and the humidity. Each experimental run in Table 2 includes the velocity measured with an anemometer at different measuring points (grid arrangement) on the inlet section, and then the inlet velocity is estimated as the mean of these measurements. Therefore, we need considerable time to complete each run, and we anticipate that we will need a couple of days to complete the entire test matrix, with two operators taking the experimental measurements. With this type of experimental arrangement, there is a new independent variable to consider: the operator that takes the measurements.

In order to remove the effect of the operator, the experimental runs can be taken in the two blocks represented in Table 2. The first block will be run by operator A and the second one by operator B. These blocks have been built considering the negative terms of the three-factor interaction term ($x_1x_2x_3$) column in block I, and its positive terms in block II. So, the blocking factor is the variable operator, and its effect is confounded by the three-factor interaction term (blocking generator). Thus, we lose the ability to obtain an accurate estimation of this three-factor interaction term (high-order interaction terms are usually negligible), but with the important benefit of having eliminated the effect of the operator variable (Blocks I and II remain orthogonal and altering the apparent effect of the three-factor interaction term with the operator effect does not change the estimate of any of the other effects).

Suppose now that it is not possible to obtain the experimental measurement for the two blocks included in Table 2. Our testing capacity is limited, and a more compact experimental design is required.

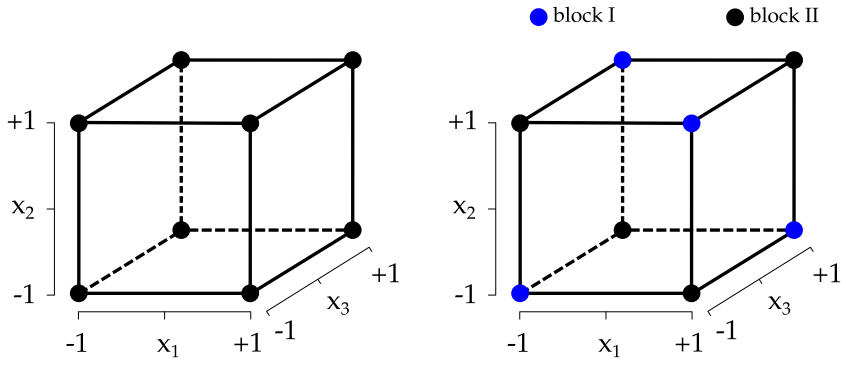

Fig. 3. Factorial design: 2^3.

In this situation, a fractional design can be selected, taking only the experimental measurements corresponding to block I (2^{3-1} fractional design; blue points in Fig. 3). This experimental arrangement allows us to run only 4 of the 8 experimental points included in the full factorial design.

Of course, this loss of information will result in the inability to estimate the three-factor interaction term by selecting only one of the blocks. This is not important because, as mentioned above, the effect of this interaction is confounded with the operator, as well as being negligible. Additionally, selecting only one of the blocks will result in the estimation of the main variables being confounded with the two-factor interaction terms (aliasing). This is not a desirable effect because the two-factor interaction terms may not be negligible, so in this case a fractional design is not recommended.

However, when the process characterized involves a high number of independent variables, the main terms are aliased by high-order interaction terms. For example, considering 5 independent variables and two blocks (the blocking generator is the five-factor interaction term), the effect of x_1 is aliased with the four-factor interaction term $x_2x_3x_4x_5$, expected to be negligible. So, fractional design allows us to construct more compact experimental designs with negligible loss of information when the process includes a large number of independent variables.

Considering the abovementioned concepts, 4 different experimental designs have been selected from the technical literature to determine the best experimental design to characterize the DSHP. The required levels for the independent variable are fixed by each design and have been selected considering the same variable range used when developing the simulated data to adjust the *"base polynomial models"*.

- Central Composite Design [24].
- Box & Behnken [25].
- Hyper-Graeco-Latin-Square [26].
- Taguchi's matrix L16b [27].

The first design, the Central Composite Design (CCD), is the most commonly used design to adjust second-order models. It is obtained by adding axial runs and replicated center points to a 2^k design, so it fixes a total of 3 or 5 levels for the independent variables. These extra points allow us to estimate the curvature effects, and adding replicated center points increases the robustness of the design to outlying observations.

Fig. 4 shows a CCD design including three independent variables in the three-dimensional space.

This figure illustrates that different distances can be selected for the extra-axial points. The CCD can be built as a face-centered design, which defines a cuboidal region with only 3 levels for the independent variables, or as a circumscribed design, which defines a spherical region including 5 levels for the independent variables. This last typology has been selected to increase the total number of levels and extend the experimental region being characterized. [23, chap. 15, Table 15.5] includes the CCD selected for a total of 5 independent variables with 49 experimental runs divided into three blocks.

The second design (Box & Behnken) is an alternative to the CCD. It requires only 3 levels for each independent variable, so it needs a lower number of experimental runs compared to the CCD. This design is built by combining two-level factorial designs with incomplete blocks in a particular manner. For example, selecting three independent variables, the Box & Behncken design includes the midpoints of edges and three replications at the center, Fig. 5. The Box & Behnken design selected for 5 independent variables is provided in [23, chap. 15, Table 15.9]. It includes 46 experimental runs.

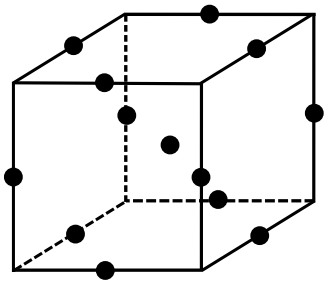

Fig. 5. Box & Behnken design.

The third design selected is the Hyper-Graeco-Latin-Square (HGLS). Ronald Fisher used it to design field experiments in agriculture. It is an orthogonal design that includes the same levels for all the independent variables. The selected HGLS, including 5 independent variables, is reported in [28, section 5.3.3.2.3]. It considers a total of 25 experimental runs.

Finally, the last design selected is a Taguchi design. This Japanese engineer has provided a lot of experimental design arrangements constructed for a different number of experimental variables and levels. They are easy to use, as it is only necessary to identify a design with the corresponding number of independent variables. The selected design was the Taguchi's matrix L16b [27,29] for 5 independent variables and 4 levels.

3.2. Comparison and selection of the most suitable experimental design

Once a proper set of experimental designs has been selected, the next step is to identify the best experimental design to characterize the DSHP. The approach used to identify it was to conduct a comparative study between these designs for the prediction of the performance in the main operating mode of the DSHP, Winter Ground. This comparative study was carried out with the IMST-ART model. Fig. 6 shows a simple diagram including the necessary steps to compare the different experimental designs with the virtual database obtained with the IMST-ART model of the unit. The main objective will be to identify the most advantageous design in terms of prediction accuracy and sample size to perform the experimental matrices to be tested.

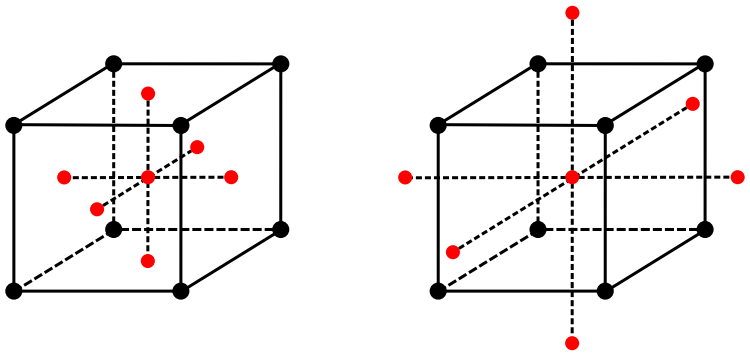

Fig. 4. Central Composite Design: Face centered (left-hand) vs Circumscribed (right-hand).

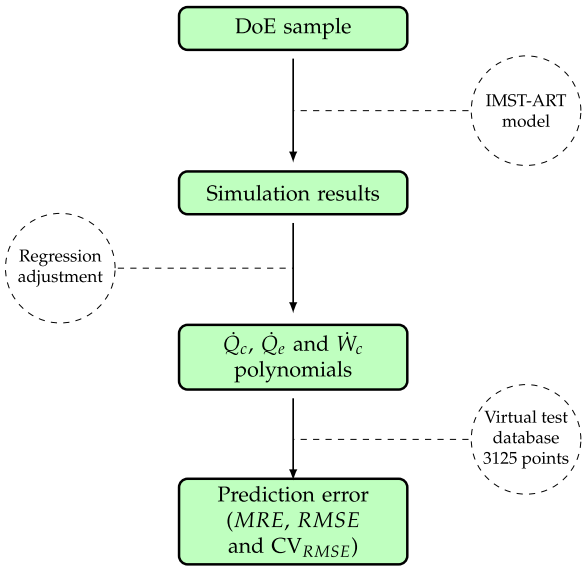

Fig. 6. DoE comparison (WG mode).

First, the simulated results were generated with the IMST-ART model for the experimental runs defined by each experimental design. Then, the *"base polynomial models"* were fitted with these simulation results (*i.e.*, with the sample defined by the experimental design).

Finally, the predictions from those fitted polynomials were compared with the virtual database – 3125 performance values in WG mode – covering the entire domain. This gave us a criterion to compare the different methodologies quantitatively and investigate the further reduction of the corresponding test matrices by taking only part of their orthogonal blocks.

The results for comparing the selected DoE arrangements are summarized in Table 3. This table shows the Maximum Relative Error (MRE), the Root Mean Square Error (RMSE), and the Coefficient of Variation of the RMSE (CV_{RMSE}) obtained for each performance parameter. As can be observed, the maximum deviation is very low for most of the methodologies, considering the small number of points in the test matrix employed to adjust the polynomials and the broadness of the 5D solution domain considered.

As can be seen, the solution provided by the CCD, taking into consideration only blocks I and III, which means utilizing only 30 test points, was highly accurate when it came to determining the response surface. Also, the HGLS provides outstanding results with only 25 points. Still, the CCD methodology was selected as the final design with orthogonal blocks I and III. The main reasons for its selection were that:

- It is a very well-established and perfectly defined methodology providing very clear and ordered test matrices.
- It allows the adjustment of second-order polynomial models such as those developed in [16].
- The sample size is adequate without involving a large number of tests.
- The addition of central points will allow, as will be seen in Section 4, the development of a new fitting methodology capable of combining simulation results with experimental results.

Just as an example, Fig. 7 shows the results of the compressor consumption polynomial model (Eq. (4)) adjusted with the CCD and Taguchi samples, clearly demonstrating how the polynomial fitted to the points defined by the CCD methodology can perfectly describe the whole response surface of 3125 points (virtual database).

The experimental test matrices built with the CCD methodology are included in the supplementary material. They were used in order to select the experimental points tested on the experimental test bench. Each of these matrices include a total of 30 experimental points excluding DHW operating modes. The matrices of these modes remove the independent variable T_{co} (user supply water temperature), reducing the total number of test points to 20. Due to DHW modes are aimed at producing domestic hot water, the value of T_{co} is expected to be constant.

However, this variable was included during the development of the *"base polynomial models"* for the DHW operating mode because data collection through simulation did not involve an excessive extra workload. Therefore, the effect of T_{co} included in the DHW polynomial models is only based on the simulated results generated with the IMST-ART model. No readjustment of this influence will be made in Section 4 for DHW modes as no experimental information is available.

3.3. Test rig

This section introduces the experimental test rig used to carry out the entire experimental campaign on the DSHP. As is described in Section 2.1, the DSHP includes three internal BPHEs and one RTPFHx, in order to work in all the operating modes described in Table 1. Therefore, the experimental test rig includes three different hydraulic loops – User, DHW, and Ground loops – and the unit is located inside a climatic chamber, which can set the required temperature and humidity conditions.

Fig. 8 shows a simple diagram of the experimental test rig and Fig. 9 some photographs of the DSHP installed in the laboratory.

The three hydraulic loops are able to set the desired return temperatures to the DSHP, working with three external PHEs and a set of 3-way valves actuated by PID controllers. These PHEs dissipate or absorb the thermal loads with three external water circuits: hot water (60 °C – Summer modes), cold water (14 °C – Winter modes), and condensation water (20 °C – specific situations).

The first hydraulic loop (User) simulates the building demand when the DSHP selects an operating mode with the User BPHE active. Then, the second loop (Ground) reproduces the ground conditions, simulating the return temperature from the borehole heat exchanger when the unit works as a geothermal HP. This hydraulic loop is not connected to the external hot water circuit. Instead, a set of three electric heating resistors compensate for the drop in temperature when the unit works in Winter mode. Finally, the third loop (DHW) sets the conditions when the unit produces DHW, simulating the DHW demand. The configuration for this loop is similar to the previous one.

Table 3
DoE methodology results: Performance prediction in WG mode.

	$\dot{Q}_c$			$\dot{Q}_e$			$\dot{W}_c$			
	MRE	RMSE	CV_{RMSE}	MRE	RMSE	CV_{RMSE}	MRE	RMSE	CV_{RMSE}	Test Points
	%	W	%	%	W	%	%	W	%	
CCD (Blocks I + III)	1.98	34.29	0.51	3.05	34.47	0.64	1.42	7.30	0.39	30
Box & Behnken	2.63	42.24	0.63	4.84	42.74	0.80	1.55	6.19	0.33	46
Hyper-Graeco-Latin-Square	1.98	35.15	0.52	3.08	34.64	0.65	1.51	7.15	0.38	25
Taguchi	2.44	43.04	0.64	4.81	42.83	0.80	6.49	23.66	1.25	16

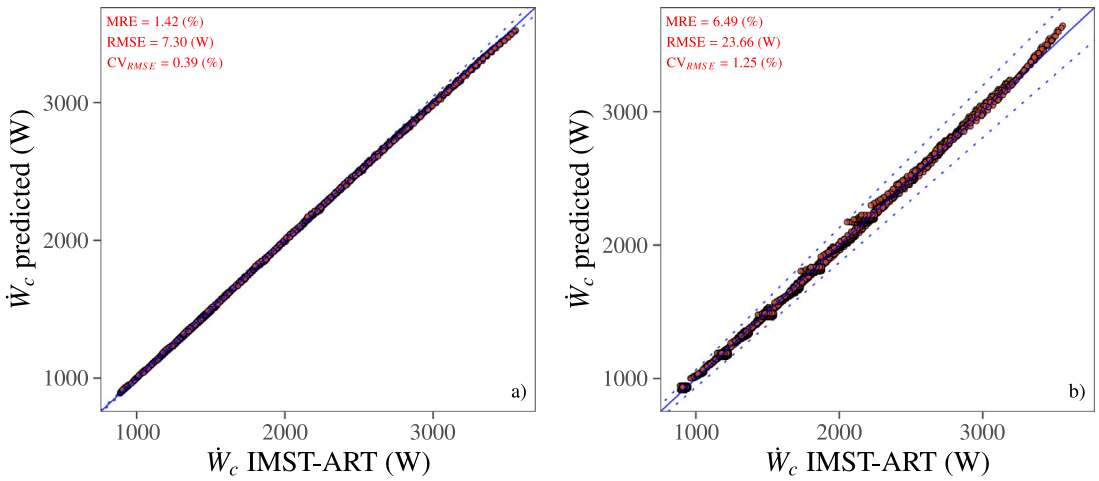

Fig. 7. WG mode: IMST-ART compressor consumption vs calculated values with the polynomial model fitted to (a) blocks I and III of CCD, and (b) Taguchi.

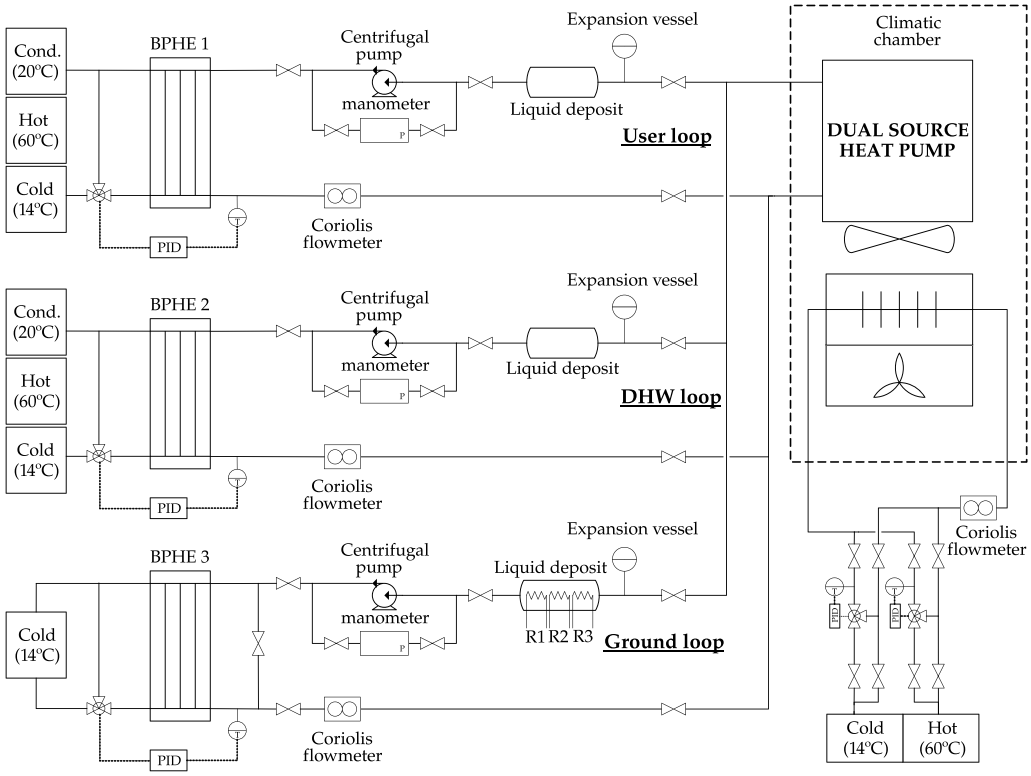

Fig. 8. DSHP experimental test rig (diagram).

The selected working fluids were water for the User and DHW loops and propylene glycol – 30% mass fraction – in the Ground loop. The rest of the elements located in the hydraulic loops are listed below:

- Hand valves ⇒ Allows the desired hydraulic loops to be connected according to the operating mode tested.
- Expansion vessels ⇒ Compensate the change in volume of the secondary fluid due to the temperature change.
- Buffer tanks ⇒ Prevent sudden changes in conditions.
- External circulation pumps ⇒ Circulate the secondary fluid.

The capacities of the heat pump were determined at the water/brine side, including the use of Coriolis flow meters to ensure high accuracy when measuring the secondary mass flow. Additionally, Resistance Temperature Detectors (RTDs) were used to measure the supply and return temperatures of the secondary fluid in each loop. Finally, 24 T-type thermocouples were placed at various positions within the refrigerant circuit to monitor and measure temperatures at the inlet/outlet points of different unit components. Two absolute pressure transmitters were also provided in the compressor suction and discharge pipes, and a power meter was fitted to measure the total power input and the compressor consumption.

Table 4 shows the model, units and location for all the sensors/actuators installed.

3.4. DSHP experimental dataset

The DSHP has been tested on the described test bench, including two experimental campaigns.

The initial campaign aimed to assess the prototype's performance and identify potential design enhancements. This set of tests mainly

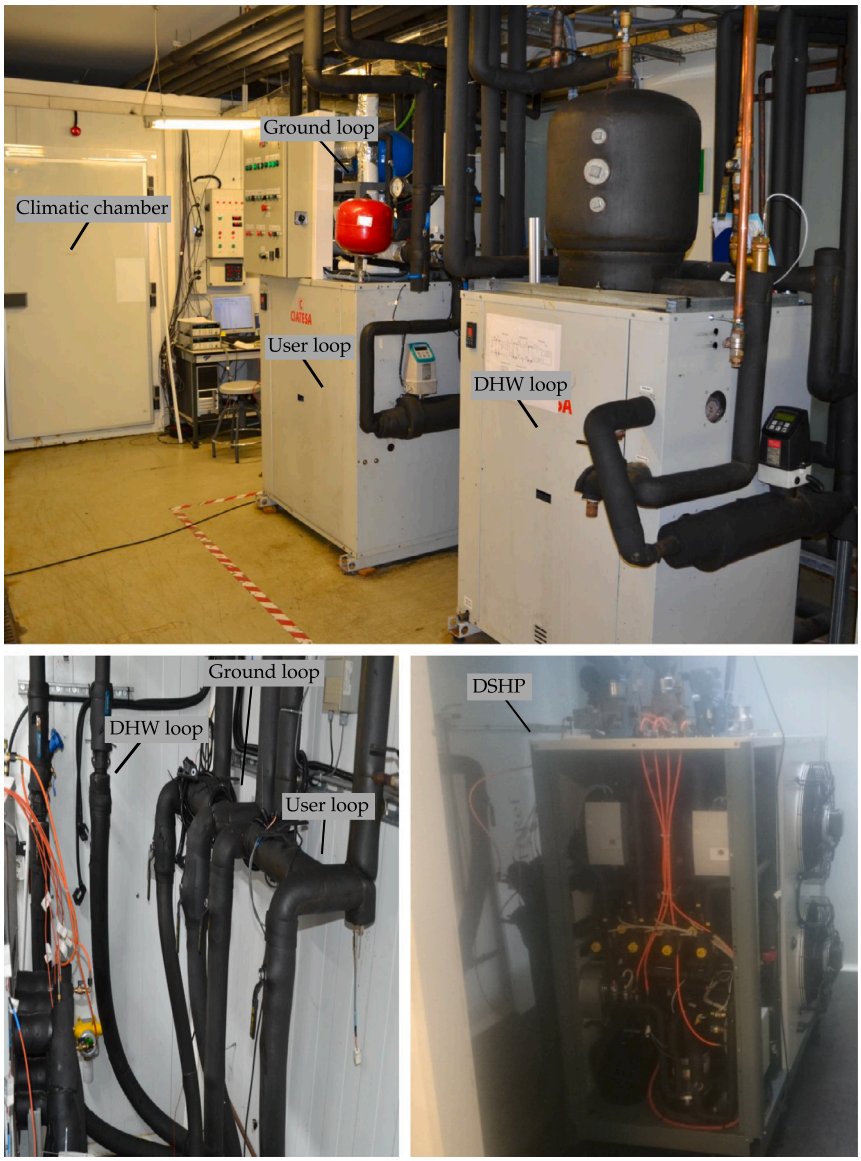

Fig. 9. Experimental test rig.

includes the nominal conditions for all the operating modes, the evaluation of the frost formation in the RTPFHx, parametric studies for the variable speed compressor and fan, the evaluation of the compressor oil return, and additional tests to check transitions between operating modes. The main conclusions of all these results are reported in [30].

Subsequently, the second experimental campaign extended test conditions for all operating modes. These experimental results were obtained to refine the *"base polynomial models"* of this unit. Section 4 describes the novel methodology established in this study for this purpose. The test conditions were defined according to the operating conditions described in [16], covering the complete working map of the DSHP and defining the test matrices according to the selected experimental design introduced in the previous section (the Central Composite Design). The data for the characterization of the unit performance at each test point had been recorded at steady-state conditions over 45 min with an interval of 5 s between measurements. Then, the experimental values for the monitored variables in each individual test were reported as the mean of all measurements recorded throughout the test duration without outliers, in order to minimize random error. The experimental tests and the corresponding error analysis for the measurements are included in the supplementary material.

Table 5 shows a summary of all the experimental test data obtained in both experimental campaigns.

Once the experimental campaign was concluded, the unit demonstrated proper functionality across all the operating modes. Only a minor issue was identified specifically in the summer modes (SG and SA). Bubbles at the liquid receiver outlet were observed, with a more pronounced effect in Summer Ground mode compared to Summer Air. In order to mitigate the bubble formation, the refrigerant charge was increased during the summer tests from the original 3 kg to 4 kg, achieving subcooling close to 1. Although the bubbles persisted, their occurrence was reduced, so a final refrigerant charge for this prototype was recommended to be set at 3.5 kg [30] (the unit employs a liquid receiver at the condenser outlet). Analysis attributed the bubbles to potential liquid flashing, likely induced by the liquid receiver's level being below the expansion valve inlet, so any pressure drop can produce the flashing and the formation of bubbles. However, the expansion valve effectively adapted to these bubbles without compromising performance. Additionally, another issue notified was that the EEV could not set the 5 K of superheat in two tests in Summer Air, and particularly in some tests of Summer Ground. In Summer Ground mode, low compressor pressure ratio and high flow rates resulted in

Table 4
Instrumentation.

Sensor/actuator	Model	Units	Measurement	Location
Thermocouple	T-type (class 1)	2	T_s ; T_d	Compressor inlet/outlet
		2	$T_{rec,in}$; $T_{rec,out}$	Inlet/outlet liquid receiver
		2	$T_{EEV,in}$; $T_{EEV,out}$	Inlet/outlet EEV
		2	$T_{coil,in}$; $T_{coil,out}$	Inlet/outlet RTPFHx (refrigerant)
		10	$T_{C1,in}$ and $T_{C1,out}$ to $T_{C5,in}$ and $T_{C5,out}$	Inlet/outlet RTPFHx circuits
		6	$T_{g,in}$; $T_{g,out}$; $T_{u,in}$; $T_{u,out}$; $T_{d,in}$; $T_{d,out}$	Inlet/outlet BPHE (refrigerant)
RTDs	PT100	6	T_{co} ; T_{ci} ; T_{eo} ; T_{ei}	Inlet/outlet BPHE (secondary)
		2	T_a [a]	Inlet RTPFHx (air side)
Pressure transducer	Rosemount 2088 (absolute)	1	P_e	Suction pressure
	Rosemount 3051 (absolute)	1	P_c	Discharge pressure
	Rosemount 3051 (relative)	1	$(P_d - P_{EEV})$	ΔP from discharge to inlet EEV
	Yokogawa (relative)	1	ΔP_{water} ; ΔP_{brine}	ΔP secondary
Humidity sensor	HUMICAP 180	1	RH	Climatic chamber humidity
Humidifier	Hygromatik HL 80	1	–	Climatic chamber
Flowmeter	Siemmens Mass 2100 DL15 (Coriolis)	1	$\dot{m}_{user}$	User hydraulic loop
		1	$\dot{m}_{dhw}$	DHW hydraulic loop
		1	$\dot{m}_{ground}$	Ground hydraulic loop
Powermeter	A2000 Multifunctional Power meter	2	$\dot{W}_{DSHP}$; $\dot{W}_c$ [b]	Connected to HP power
Pitot	Vaisala HMP141A	1	$p_{total} - p_{static} \Rightarrow v_a$ (Air side)	Air velocity (RTPFHx outlet)
3-way valve	SKD62 Landis & Steafa	1	–	User hydraulic loop
		1	–	DHW hydraulic loop
		1	–	Ground hydraulic loop
PID	KS 90-1 (PMA)	1	–	User hydraulic loop
		1	–	DHW hydraulic loop
	Watlow 96	1	–	Ground hydraulic loop
	RWX-62 Siemmens	2	–	Climatic chamber
Datalogger	Agilent 34972	2	–	Room

[a] Average value.
[b] This measurement includes the inverter consumption.

Table 5
DSHP experimental campaign.

Test	Summer Air	Summer Ground	DHW User	Winter Air	Winter Ground	DHW Air	DHW Ground	Total test points
Nominal conditions	1	1	1	2	2	2	2	
Variation f_c (User 40/45)	–	–	–	4	4	–	–	
Variation f_c (User 30/35)	–	–	–	4	4	–	–	
Variation f_{fan}	–	–	–	3	–	–	–	
Frost formation	–	–	–	4	–	–	–	227
Test matrices (DoE)	30	20	20	30	30	20	20	
Winter Ground as DHW	–	–	–	–	3	–	–	
Double evaporator (WA/WG)	–	–	–	4	–	–	–	
Extra test	1	1	2	–	6	3	3	

full valve opening, impacting superheat control and reducing EER. This phenomenon was identified mainly in Summer Ground mode and attributed to the combination of bubbles and low-pressure ratios. Since this problem should be corrected by improvements in the design of this first prototype, these tests have not been considered when refitting the polynomial models to the experimental data described in the next section.

Finally, it was also verified in the laboratory that the transition between operating modes was adequate. In this sense, when the unit changes from season (Winter modes to/from Summer modes), the compressor stops. Then, after a short period, the start-up into the desired operating mode is performed: First, valves open to their corresponding state, and then the compressor starts up and accelerates as in any inverter-driven unit. Subsequently, when the unit operates in the same season, the same procedure is consistently applied across all mode changes.

The programmed sequence for mode transitions in the same season involves:

- Slow down the compressor speed to the minimum frequency.
- A brief unit operation during a changing delay time.
- Simultaneous opening of solenoid valves for the new mode (*e.g.*, SA2 and SAS in Fig. 1 for Winter-air mode), allowing parallel operation of evaporators (same procedure when switching condensers in DHW modes).
- Maintain parallel operation during a contemporary time for a short duration.
- Close solenoid valves related to the departure mode (either on the discharge or suction and expansion).
- Once again, the unit continues operating in the newly selected mode by increasing the compressor speed to the desired one.

From the mode change analysis, the only potential problem was the possible migration of liquid refrigerant to the compressor suction during some transitions, such as from Summer Air to DHW Air. In order to do it, the unit operates in a similar way to the previous one described. This means that to change from Summer Air to DHW Air, the unit has to go first through the working mode DHW User mode. The next step is to change the evaporator from the User BPHE to the Air source. In this sense, the unit changes from condensing at the RTPFHx coil to condensing in the DHW BPHE, so that all the refrigerant stored in the RTPFHx coil must migrate towards the liquid receiver going through the compressor when it is switched into the evaporator in

the new operating mode. Similar circumstances arise during the mode transition from Summer Ground to DHW Ground. However, the impact is less critical because the Ground BPHE contains a smaller liquid quantity than the RTPFHx coil. Extensive studies, including camera monitoring, confirmed some liquid refrigerant entering the compressor. Fortunately, the compressor design, in which the refrigerant enters the crankcase for cooling, protects against damage from liquid droplets. The manufacturer, informed of this temporary liquid ingress, recognizes that minimal refrigerant ingress for a short period of time does not cause any damage to the compressor.

Therefore, during the review of switching between modes, it was possible to verify that the unit operates properly during all possible transitions. Continuous monitoring of oil return, bubble appearance at the liquid sight glass, and all measurements aimed to detect potential problems that could result in failures or component deterioration were done. No abnormal vibrations, temperature overshoots or issues were identified, and all transitions occurred smoothly.

After concluding how the experimental matrices were performed, the test rig description, and summarizing the DSHP experimental results, subsequent sections detail the new fitting methodology and compare prediction errors for the *"corrected polynomial models"*.

4. New fitting methodology for empirical models

This section explains how to conduct the final adjustments to the polynomial models using the experimental tests and the new fitting approach introduced in this work. It is important to remember that the *"base polynomial models"* were obtained using a virtual database – 3125 simulation points for each operating mode – including the working maps of the DSHP as simulated results and generated with a detailed model of the unit in the simulation software IMST-ART. Consequently, these polynomial models include the following prediction errors:

- Deviation between the adjusted regression model and the IMST-ART model.
- Deviation between the IMST-ART model and the experimental results.

Therefore, this final readjustment using the experimental results is necessary in order to reduce the prediction errors in the polynomial models.

The readjustment uses the following information:

- The *"base polynomial models"* fitted with the IMST-ART-generated virtual database.
- The experimental results of the samples reported in this work and defined with the selected experimental design, the Central Composite Design (Section 3.2).

However, *"how do we go about readjusting the polynomial models correctly?"*

One option is to take the same functional produced with the virtual database and readjust it directly with the experimental data. This involves simply recalculating the model's regression coefficients while using the same polynomial expression.

Taking the WG operating mode as an example to explore this possibility, Table 6 shows the regression model obtained for the $\dot{Q}_c$ prediction adjusted with the 3125 points of the virtual database (left column) and the 30 experimental points from the CCD (right column).

As reported in [16], for the *"base polynomial models"*, a transformation was applied to the response variable, defining a regression model for $\dot{Q}_c/f_c$. The errors in Table 6 – MRE, RMSE and CV_{RMSE} – are reported as the prediction error in $\dot{Q}_c$. The model on the left is calibrated using the simulation data and reports the errors for predicting the 30 experimental points obtained in WG mode. The model on the right uses the same polynomial model but directly fits the regression coefficients to the experimental points, also reporting the error for $\dot{Q}_c$.

As we can see from the results, the virtual database-adjusted model has an MRE = 5.6%, an RMSE = 145 W and a CV_{RMSE} = 2.1% for the prediction of the 30 experimental points from the CCD. This is a relatively low prediction error, meaning the IMST-ART model in itself produces good prediction results, and the regression model does not introduce significant deviations.

The model adjusted directly with the experimental data, on the other hand, gives a lower prediction error, with an MRE = 2.1%, an RMSE = 59.2 W and a CV_{RMSE} = 0.88%. Though it should be noted that many of the regression coefficients are non-significant and do not always maintain the same sign when compared to the virtual database-adjusted regression coefficients. The latter can be checked in Table 6, where different stars are attached to the regression coefficients according to its *p-value*. A *p-value* > 0.05 supports the null hypothesis for the regression coefficient, suggesting its removal from the regression model.

Reviewing the values of the regression coefficients, one can see that, for example, the T_{co} coefficient changes from −1.003e+01 to 4.673e+00. Generally speaking, a change in the sign of the coefficient, and therefore its tendency as a predictor, does not make sense if we assume that the points generated in the virtual database are obtained with an accurate model and are unaffected by experimental uncertainties. This arbitrary tendency to modify the sign of the regression coefficients coupled with the fact that many of them are non-significant was also observed for the $\dot{W}_c$ and $\dot{Q}_e$ models, regardless of which operating mode is selected.

One possible explanation could be the large difference in the number of points used in the adjustment. It is important to highlight that the virtual database-adjusted polynomials include a full factorial design at five levels for the five independent variables. This equates to a total of 3125 points compared to the 30 points selected in the CCD.

Even though these 30 points were carefully selected in order to obtain as much experimental information as possible, this selection is unable to produce a model homologous to the *"base polynomial model"*. In an ideal situation, the tendencies would be the same for all the regression coefficients. If, furthermore, we consider that many of the coefficients have a *p-value* > 0.05 when adjusting with the experimental data, then this seems to indicate that we should contemplate a more compact model when using the experimental sample from the CCD to get a model homologous to the virtual database-adjusted model.

As such, we can conclude that it would be ill-advised to adjust the model's regression coefficients directly with the experimental data. However:

1. *"Can the information from the virtual database be combined with the experimental results?"*
2. *"Can we improve the prediction error in the models without substantially changing the models obtained with the virtual database?"*

A second option, and the one finally chosen in this work, is to keep the virtual database-adjusted model, including the values for the regression coefficients, and then readjust using the experimental data.

The idea is to combine the simulation results – where the complete maps of the unit have been generated covering the entire working range and including a large number of points – with the points obtained experimentally and located according to the CCD methodology. For this purpose, a new 2-step fitting methodology has been developed to obtain the *"corrected polynomial models"*. In the first step, the working maps must be generated by simulation, the most suitable functional for the polynomial models is analyzed and selected, and the regression coefficients are fitted to the simulation data. This part was covered in the previous publication [16]. Subsequently, the experimental matrices must be shaped using the CCD, and this experimental information is collected to perform the refitting of the model in a second step.

Table 6
WG: $\dot{Q}_c/f_c$ model adjusted with the virtual and experimental database.

	$\dot{Q}_c/f_c$ (W/Hz) (virtual database)	$\dot{Q}_c/f_c$ (W/Hz) (experimental database)
$(Int.)$	4.617e+03 (±7.31e+01)***	2.149e+02 (±3.44e+03)
$(T_{co}{}^2)$	9.011e−03 (±5.43e−04)***	6.477e−03 (±2.12e−02)
T_{co}	−1.003e+01 (±3.65e−01)***	4.673e+00 (±1.50e+01)
$(T_{eo}{}^2)$	4.359e−02 (±4.09e−04)***	4.623e−02 (±1.81e−02)***
T_{eo}	−2.405e+01 (±2.62e−01)***	−9.982e+00 (±1.29e+01)
dT_c	2.669e−01 (±8.87e−03)***	−2.879e−01 (±3.14e−01)+
dT_e	8.238e−01 (±9.44e−03)***	6.423e−01 (±3.16e−01)***
f_c	2.826e−01 (±5.87e−02)***	1.897e+00 (±3.55e+00)
$(1/f_c)$	−1.275e+02 (±1.37e+01)***	1.159e+03 (±8.04e+02)**
$T_{co}\times T_{eo}$	1.278e−02 (±4.27e−04)***	−3.444e−02 (±2.64e−02)*
$T_{eo}\times f_c$	−1.270e−03 (±2.14e−04)***	−5.405e−03 (±1.29e−02)
Num.Obs.	3125	30
R2 Adj.	0.999	0.995
MRE (%)	5.603[d]	2.071
RMSE (W)	145.119[d]	59.187
CV_{RMSE} (%)	2.147[d]	0.876
Range (W)	[2415, 13500]	[4293, 9988]

[a] + p < 0.1, * p < 0.05, ** p < 0.01, *** p < 0.001;
[b] Temperatures (K);
[c] Compressor frequency (Hz);
[d] MRE, RMSE and CV_{RMSE} are calculated with respect to the experimental data and $\dot{Q}_c$ values.

The readjustment conducted in the second step employs the partial derivatives of the main terms (linear terms) and the value of the response variable at the CCD center point.

To simplify the explanation and represent it in a 3D graph, let us consider using this new method to readjust a model for a response variable, y, that is only dependent on two independent variables, x_1 and x_2.

This gives us an initial linear model (Eq. (5)):

$$y = (x_1, x_2) = f(x_1, x_2) \tag{5}$$

This model would be adjusted with the virtual database. In this case, as it only depends on two independent variables, we can create a 3D graph of this model, commonly called a response surface (Fig. 10).

Fig. 10 shows the response surface for the model $y(x_1, x_2)$ and the tangent plane at the point $y_0(x_{10}, x_{20})$. This point should be taken as the center point defined in the CCD.

The tangent plane at $y_0(x_{10}, x_{20})$ derives from the equation:

$$z(x_1, x_2) = y_0(x_{10}, x_{20}) + \sum_{i=1}^{2} \left.\frac{\partial y}{\partial x_i}\right|_0 \cdot (x_i - x_{i0}) \tag{6}$$

To avoid having to modify the response surface, and while also readjusting with the experimental data, the following correction can be applied:

Subtracting the tangent plane equation from the original model for response variable y, then reintroducing it but while including the correction terms (k_0, k_1, k_2), gives us Eq. (7):

$$y^*(x_1, x_2) = k_0 \cdot y_0(x_{10}, x_{20}) + \left(\sum_{i=1}^{2} k_i \cdot \left.\frac{\partial y}{\partial x_i}\right|_0 \cdot (x_i - x_{i0})\right) + \underbrace{\left[y(x_1, x_2) - y_0(x_{10}, x_{20}) - \left(\sum_{i=1}^{2} \left.\frac{\partial y}{\partial x_i}\right|_0 \cdot (x_i - x_{i0})\right)\right]}_{\delta(x_1, x_2)} \tag{7}$$

By simplifying and rearranging terms, Eq. (8) is obtained:

$$y^*(x_1, x_2) = y(x_1, x_2) + \left(\sum_{i=1}^{2} (k_i - 1) \cdot \left.\frac{\partial y}{\partial x_i}\right|_0 \cdot (x_i - x_{i0})\right) + (k_0 - 1) \cdot y_0(x_{10}, x_{20}) \tag{8}$$

Considering that $y(x_1, x_2)$ is a linear function, the new response variable $y^*(x_1, x_2)$ will also be a linear function. Therefore, coefficients

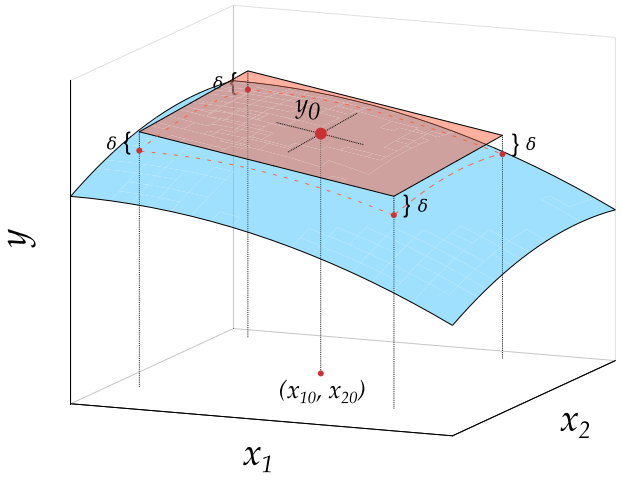

Fig. 10. Response surface y (blue) and tangent plane (orange) at the point y_0.

k_0, k_1, and k_2 could be adjusted to the experimental data from the CCD by linear regression, where $y^*(x_1, x_2)$ is the new model adjusted to the experimental data. The function $y(x_1, x_2)$ is previously established through a polynomial fit using simulation results. Computing partial derivatives is straightforward, and the coordinates, along with the value of the CCD center point, denoted as x_{10}, x_{20}, and y_0, are well-defined.

The method described above applies a readjustment without deforming or modifying the response surface; it merely changes its position. Coefficients k_1 and k_2 mean the response surface can be rotated around the x_1 and x_2 axes, taking the CCD center point y_0 as an anchor point. The term k_0 also adds a further degree of freedom for making corrections by raising or lowering the response surface in the y axis.

Regarding to the expected value for coefficients k_1 and k_2, performing the regression adjustment will return positive values close to 1 if only small corrections are required. This will only occur if the model used to generate the virtual database has a low prediction error. If the coefficients are negative, it indicates a poor fit of the model used for the simulated results or possibly a measurement error in the experimental points due to the instruments' uncertainty.

In the next step, we take an arbitrary function, $y = 60 - 0.03x_1^2 - 0.06x_2^2 + 2x_2$, and a center point at the coordinates $x_{10} = x_{20} = 10$ to illustrate how this new fitting approach works:

Example 1: Experimental readjustment

Polynomial model:

$$y = 60 - 0.03x_1^2 - 0.06x_2^2 + 2x_2$$

$$\left.\frac{\partial y}{\partial x_1}\right|_0 = -0.06x_{10} = -0.6$$

$$\left.\frac{\partial y}{\partial x_2}\right|_0 = 2 - 0.12x_{20} = 0.8$$

CCD center point:

$$x_{10} = 10$$

$$x_{20} = 10$$

$$y_0 = 71$$

Polynomial model adjusted:

$$y^* = y + (k_1 - 1) \cdot \left.\frac{\partial y}{\partial x_1}\right|_0 \cdot (x_1 - x_{10}) + (k_2 - 1) \cdot \left.\frac{\partial y}{\partial x_1}\right|_0 \cdot (x_2 - x_{20}) + (k_0 - 1) \cdot y_0$$

$$y^* = y + (k_1 - 1) \cdot (-0.6) \cdot (x_1 - 10) + (k_2 - 1) \cdot 0.8 \cdot (x_2 - 10) + (k_0 - 1) \cdot 71$$

Fig. 11 shows how incorporating some arbitrary values for the set of coefficients k_i, presumably obtained from the linear regression adjustment to a set of experimental data, repositions the response surface in Example 1 depending on the values used for k_i. The blue surface represents the original model $y(x_1, x_2)$, and the orange surface is the model readjusted with the experimental data $y^*(x_1, x_2)$.

The top left and right graphs show the effect of readjusting the k_1 or k_2 terms only, allowing the response surface to be rotated about the x_1 and x_2 axes and center point y_0. The bottom left graph reveals a slight, constant vertical difference between the two surfaces upon adjusting with k_0 and, lastly, the bottom right graph shows the readjustment using the three coefficients k_i.

This method can be applied regardless of the number of independent variables included in the model. Rearranging Eq. (8) and taking the general case of n independent variables in the model leads to the general equation:

$$y^*(x_1, \ldots, x_n) = y(x_1, \ldots, x_n) + \left(\sum_{i=1}^{n}(k_i - 1) \cdot \left.\frac{\partial y}{\partial x_i}\right|_0 \cdot (x_i - x_{i0})\right) + (k_0 - 1) \cdot y_0(x_{10}, \ldots, x_{n0}) \quad (9)$$

We can now appreciate how the use of such readjustment means we can take advantage of both simulated results and experimental tests when adjusting an empirical model.

For the DSHP analyzed in this work, conserving the response surface generated with a full factorial of 3125 simulated points, we have produced a robust model adjusted throughout the experimental domain, thus ruling out the possibility of extrapolation errors. What is more, the possible deviation in the simulated data used for the adjustment with respect to the experimental results is subsequently corrected using the new readjustment methodology. This means we can even improve the results from the polynomial models compared to the original model in IMST-ART.

Returning to the $\dot{Q}_c$ model presented in Table 6 and readjusting according to the aforementioned method, we obtain the values reported in Table 7 for the adjustment coefficients k_i.

Table 7
WG: $\dot{Q}_c$ model readjusted with the experimental database.

	$\dot{Q}_c^*$ (W)
$\dot{Q}_{c0}$	1.012e+00 (±5.66e−03)***
$k_1(x_1 = f_c)$	9.997e−01 (±3.33e−02)***
$k_2(x_2 = T_{eo})$	1.070e+00 (±4.47e−02)***
$k_3(x_3 = dT_e)$	7.679e−01 (±5.68e−01)*
$k_4(x_4 = T_{co})$	7.735e−01 (±2.14e−01)***
Num.Obs.	30
R2 Adj.	1.000
MRE (%)	3.543
RMSE (W)	91.488
CV_{RMSE} (%)	1.354
Range (W)	[4293, 9988]

[a] + p < 0.1, * p < 0.05, ** p < 0.01, *** p < 0.001;
[b] Temperatures (K);
[c] Compressor frequency (Hz).

These coefficients were obtained by first taking the $\dot{Q}_c/f_c$ model shown in Table 6 adjusted with the virtual database (left column). Then, we multiplied the $\dot{Q}_c/f_c$ model by f_c to get a new polynomial expression, eliminating the transformation carried out on the response variable. Next, we calculated the partial derivatives concerning each of the independent variables in this new polynomial for $\dot{Q}_c$ and applied Eq. (9). Lastly, considering k_0, k_1,…, k_5 to be adjustment coefficients, we applied a regression adjustment using the 30 experimental points from the CCD. The 30-point CCD in WG includes four replicas for the center point and the experimental readjustment is made while taking into account the values of $\dot{Q}_{c0}$, f_{c0},…, that is, the mean of the experimental results for the four center point replicas.

As we can see, the readjustment leads to an improvement in the model's prediction error. The MRE is just 3.5% instead of 5.6%, the RMSE is 91.5 W compared to 145 W and the CV_{RMSE} is 1.35% instead of 2.15%, thus improving on the prediction error for the original regression model and the IMST-ART model. Therefore, we have developed a new technique to translate detailed models into easily programmable

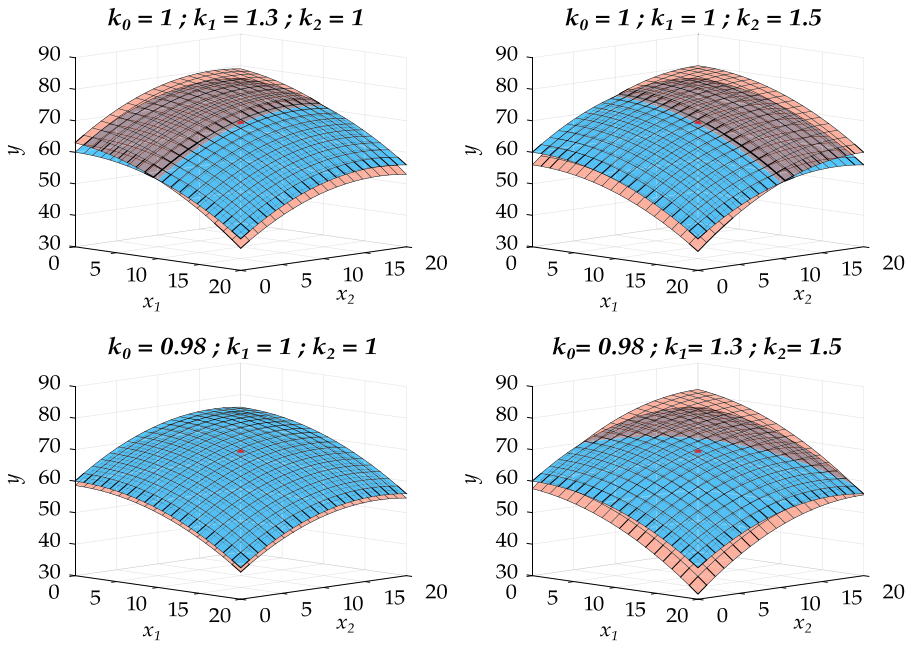

Fig. 11. Experimental readjustment for different values of k_i. Original model (blue surface) and readjusted model (orange surface).

and more accurate empirical models, allowing us to improve prediction errors significantly in cases where the detailed model describes the physics of the process only in general terms.

With regard to the values of the resulting coefficients, it is notable that they are all positive and close to 1, so the readjustment causes a slight repositioning of the response hypersurface and does not change the sign and, therefore, the tendency of the coefficients. A negative value was only returned in the case of the predictor dT_c, which indicates that the trend of the condenser capacity with dT_c in the experimental results is not the same as the one obtained in the simulated results.

This negative value was confirmed as being due to experimental uncertainty. The condenser capacity is calculated by means of the secondary balance, obtaining lower water flow rates compared to the evaporator and therefore increasing the experimental uncertainty. This, coupled with the fact that the capacity has very little dependence on the variable dT_c (as was reported in [16]), is responsible for this change in tendency in the experimental readjustment. Therefore, since the detailed model in IMST-ART is insensitive to the measurement uncertainties and given this coefficient exercises an insignificant correction on the model, dT_c was disregarded in the experimental readjustment by eliminating the factor k_5.

Having finished the description of how to readjust the models to the experimental data, the final results are summarized in the next section.

5. Final results

Appendix A includes the $\dot{W}_c$, $\dot{Q}_c$ and $\dot{Q}_e$ models for all the operating modes summarized in:

- A first table for each operating mode contains the $\dot{W}_c/f_c$, $\dot{Q}_c/f_c$ and $\dot{Q}_e/f_c$ polynomial models adjusted with the virtual database (*"base polynomial models"*). In this table, the polynomial model prediction errors (MRE, RMSE and CV_{RMSE}) are calculated with respect to the simulation results, thus reconverting the values for the estimation of $\dot{W}_c$, $\dot{Q}_c$ and $\dot{Q}_e$.
- A second table is also attached with values for the k_i adjustment coefficients obtained from the readjustments with the experimental data. In this case, the prediction errors are expressed with respect to the experimental results. Thus we can obtain the final regression models based on these two tables and Eq. (9) (*"corrected polynomial models"*).
- Lastly, a series of figures is included as a visual comparison of the adjustment of these models, the model adjusted with the virtual database and the final regression model readjusted with the experimental data.

Regarding the values obtained for the k_i coefficients, the water-to-water and brine-to-water modes obtained positive values close to 1. The DHW User, DHW Ground, and Summer Ground modes also obtained a negative value in the k coefficient for the predictor dT_c; therefore, as in Winter Ground mode, it has been removed from the experimental readjustment. Additionally, the Summer Ground mode only includes the k_i coefficients for the main predictors f_c, T_{eo} and T_{co}, due to the rest of coefficients became negative. This is because, as mentioned in Section 3.4, the EEV was not able to set the 5 K of superheat in some tests, with the presence of bubbles upstream of the EEV. Therefore, only 8 experimental points from the total of the 30 tests are available for the experimental readjustment.

Then, regarding the air modes, they obtained similar results to the previous ones. Only, the k coefficient for the predictor f_{fan} in Winter Air and DHW Air modes gets a higher value for the readjustment of $\dot{W}_c$, and probably indicates that the fan characterization included in the IMST-ART model could be improved. However, this coefficient has the same trend with a positive value, and therefore, it has not been removed. Finally, some values of the k_i coefficients for the predictors dT_c and dT_e obtained negative values in the air modes, due to the experimental uncertainty. They have also been removed from the experimental readjustment.

Once the final models have been included in Appendix A, we can see that all the fitted models have low prediction errors. As a summary, Table 8 includes the MRE, RMSE and CV_{RMSE} of the empirical models built for the prediction of $\dot{W}_c$, $\dot{Q}_c$ and $\dot{Q}_e$ in the 7 operating modes. In order to be in a position to assess whether the experimental readjustment improves the prediction errors, this table includes the prediction error of the original models built with the virtual database, and the models readjusted with the methodology described in Section 4. Both errors refer to the prediction of the experimental data.

Table 8
Prediction errors for the final polynomial models.

	$\dot{W}_c$		$\dot{Q}_c$		$\dot{Q}_e$	
	PM[a]	PMA[b]	PM[a]	PMA[b]	PM[a]	PMA[b]
Winter Ground						
MRE (%)	2.850	2.131	5.603	3.543	4.589	3.351
RMSE (W)	18.181	13.488	145.119	91.488	124.549	77.069
CV_{RMSE} (%)	0.970	0.720	2.147	1.354	2.317	1.434
Summer Ground						
MRE (%)	10.794	1.087	6.979	2.235	5.735	2.122
RMSE (W)	32.104	6.612	261.855	83.672	186.385	80.695
CV_{RMSE} (%)	2.989	0.616	2.943	0.940	2.378	1.029
DHW Ground						
MRE (%)	5.228	1.756	6.862	4.721	4.559	2.100
RMSE (W)	71.717	18.918	257.677	129.369	149.604	64.792
CV_{RMSE} (%)	3.512	0.927	3.449	1.732	2.415	1.046
DHW User						
MRE (%)	5.051	1.505	3.791	2.776	5.775	1.672
RMSE (W)	71.294	15.290	125.186	111.968	273.251	56.137
CV_{RMSE} (%)	3.406	0.730	1.351	1.208	3.625	0.745
Winter Air						
MRE (%)	1.673	1.966	12.379	2.783	13.305	3.325
RMSE (W)	13.864	12.000	621.020	84.117	523.350	83.303
CV_{RMSE} (%)	0.726	0.629	8.085	1.095	8.177	1.302
Summer Air						
MRE (%)	6.523	1.225	6.854	2.791	6.820	2.399
RMSE (W)	71.757	10.685	398.599	88.533	327.614	66.111
CV_{RMSE} (%)	4.377	0.652	4.335	0.963	4.053	0.818
DHW Air						
MRE (%)	4.597	1.681	15.202	4.378	16.962	5.854
RMSE (W)	62.919	17.653	899.789	138.660	813.285	166.491
CV_{RMSE} (%)	3.026	0.849	10.646	1.641	11.474	2.349

[a] Polynomial model adjusted with the virtual database and predicting the experimental data.
[b] Polynomial model readjusted with the experimental data.

We can see that the prediction errors decrease in the 7 operating modes. Therefore, the empirical models improve the prediction errors of the IMST-ART model, with a value of 1%–3% of MRE in most models.

Moreover, these polynomial equations are easy to implement, regardless of the programming or simulation tool selected. Depending on the modeling approach selected, other types of modeling approaches could require complex equation converge solving. In this case, the only requirement is to pre-adjust the regression coefficients of the polynomial by using experimental and simulated data according to the methodology introduced in this work. Due to the corrected polynomials are still linear functions, they are easy to implement in any simulation software or even in the unit controller.

Finally, Appendix B, includes an example of how to recompose the model with the summarized data provided in Appendix A for the $\dot{W}_c$ prediction in Winter Ground mode (Example 2).

6. Conclusions

This paper explores modeling geothermal and aerothermal heat pumps and chillers using empirical models to accurately predict unit performance across the entire working map (development of map-based models). A previous study [16] detailed the construction of polynomial models for characterizing seven operating modes in a Dual Source Heat Pump derived from comprehensive working maps generated through simulation. The current work focuses on obtaining experimental data in the laboratory, defining an optimal strategy to perform experimental matrices, and describing a new adjustment methodology to update the models reported in [16] using both simulated and empirical information. The main conclusions of this work are as follows:

- The new prototype of DSHP analyzed in this work operates with R32 refrigerant and includes a variable speed compressor, which gives full capabilities for efficient modulating operation. The unit has turned out to be fully reliable and has a smooth, simple, and fully automatic operation. It has been designed and thoroughly tested at the laboratory of the IUIIE with very accurate instrumentation by using a proper experimental test bench.
- The DSHP has the capability to choose from seven operating modes, involving the selection between heat pump or chiller operation and the utilization of geothermal and aerothermal loops as sources. Therefore, this study demonstrates the process of achieving a suitable characterization through the utilization of empirical models for the primary heat pump and chiller technologies present in the market.
- This unit allowed the generation of a large amount of experimental data with a total of 227 test points. Thanks to the unit's ability to select different heat sources, all the experimental data generated include the performance of the main heat pump technologies – Air Source and Ground Source Heat Pumps – including data for an extended range of boundary conditions and also different operating modes (DHW application, heating mode, and cooling mode).
- A testing campaign following a full factorial plan would require a huge number of test points, *e.g.*, 3125 points with 5 levels for each independent variable. Therefore, some Design of Experiments methodology (DoE) must be applied to reduce the test matrix to a reasonable size.
- The IMST-ART model allowed the evaluation of different DoE methodologies, defining which DoE methodology leads to a good compromise between the number of points for the fitting of the surface and the accuracy of the prediction. Thus, the Central Composite Design (CCD) is a suitable option, requiring 30 test points respectively and allowing a very good characterization of the unit performance across the whole domain. This design was

used to perform the experimental test matrices. They include the major part of the 227 experimental points tested.
- The polynomials generated from the virtual database and reported in [16] were finally fitted using the experimental points defined by the CCD and a new methodology developed in this work. The fitting methodology used has proved adequate in the sense of being able to combine the extensive information obtained from the simulated data together with the experimental data.
- The developed polynomials were compared with the experimental performance data and provided a good prediction. The prediction error is very small, across the entire 5D domain: $< 2\%$ for the energy consumption and $\approx 3\%$ for the condenser and evaporator capacities.
- A novel technique has been developed to transform detailed models into easily programmable and more accurate empirical models, leading to a substantial improvement in prediction errors, especially when the detailed model provides a generalized description of the process physics characterized. However, this new technique has only been tested on the experimental data reported in this work, and further investigation is necessary to verify its general applicability in the modeling of other systems and units.
- The generation of the complete working maps by simulation, together with the experimental readjustment, allows the elimination of undesired effects of empirical modeling, such as overfitting or extrapolation and interpolation errors. The full factorial generated by simulation allows the most appropriate polynomial expressions to be analyzed and fixed. Subsequently, the new refitting methodology introduced in this work allows the simulated information to be efficiently combined with experimental data obtained in the laboratory. This allows for minimizing possible errors between the detailed model used to generate the working maps and better capture the real physics of the characterized process.

CRediT authorship contribution statement

Javier Marchante-Avellaneda: Writing – review & editing, Writing – original draft, Visualization, Validation, Software, Methodology, Investigation, Formal analysis, Data curation, Conceptualization. **Emilio Navarro-Peris:** Writing – review & editing, Supervision, Resources, Formal analysis, Conceptualization. **Francisco Barceló-Ruescas:** Writing – review & editing, Resources, Investigation, Conceptualization. **Yang Song:** Writing – review & editing, Investigation, Conceptualization.

Data availability

Data will be made available on request.

Acknowledgment

The present work has been supported by the European Community Horizon 2020 Program for European Research and Technological Development (2014–2020) inside the framework of the project 656889 – GEOTeCH (Geothermal Technology for Economic Cooling and Heating), by the project "DESCARBONIZACIÓN DE EDIFICIOS E INDUSTRIAS CON SISTEMAS HÍBRIDOS DE BOMBA DE CALOR", funded by the "Ministerio de Ciencia e Innovación", MCIN, Spain, with code number: PID2020-115665RB-I00 and by the postdoctoral fellowship funded by "Universitat Politècnica de València" inside the program "Ayudas para Contratos de acceso de personal investigador doctor (PAID-10-23)".

Many thanks as well to the late Dr. José Miguel Corberán, without whom this work would never have been possible. Sadly, Dr. José Miguel Corberán passed away in July of 2022. I wish to give my wholehearted support to José Miguel's family. I hope we did you proud.

Appendix A. Empirical models DSHP

This appendix includes the $\dot{W}_c$, $\dot{Q}_c$ and $\dot{Q}_e$ models for all operating modes summarized in:

- A first table for each operating mode contains the $\dot{W}_c/f_c$, $\dot{Q}_c/f_c$ and $\dot{Q}_e/f_c$ polynomial models adjusted with the virtual database. In said table, the polynomial model prediction errors (MRE, RMSE and CV_{RMSE}) are calculated with respect to the simulation results, thus reconverting the values for the estimation of $\dot{W}_c$, $\dot{Q}_c$ and $\dot{Q}_e$. See Tables A.1, A.3, A.5, A.7, A.9, A.11 and A.13.
- A second table is also attached with values for the k_i adjustment coefficients obtained from the readjustments with the experimental data. In this case, the prediction errors are expressed with respect to the experimental results. Thus we can obtain the final regression models based on these two tables and Eq. (9). See Tables A.2, A.4, A.6, A.8, A.10, A.12 and A.14.
- Lastly, a series of figures is included as a visual comparison of the adjustment of these models, the model adjusted with the virtual database and the final regression model readjusted with the experimental data (see Figs. A.1–A.7).

A.1. Winter ground

CCD central point:

$\dot{W}_{c0}$ = 1856.612 (W) $\dot{Q}_{e0}$ = 5276.218 (W) T_{eo0} = 273.184 (K)

T_{co0} = 318.272 (K) $\dot{Q}_{c0}$ = 6658.974 (W) f_{c0} = 50 (Hz)

dT_{e0} = 4.972 (K) dT_{c0} = 5.078 (K)

Partial derivatives at CCD center point:

$\left.\frac{\partial \dot{W}_c}{\partial f_c}\right|_0$ = 5.186e+01 $\left.\frac{\partial \dot{W}_c}{\partial dT_c}\right|_0$ = −1.304e+01 $\left.\frac{\partial \dot{Q}_c}{\partial T_{co}}\right|_0$ = −3.992e+01 $\left.\frac{\partial \dot{Q}_e}{\partial T_{co}}\right|_0$ = −6.668e+01

$\left.\frac{\partial \dot{W}_c}{\partial T_{eo}}\right|_0$ = 7.033e+00 $\left.\frac{\partial \dot{Q}_c}{\partial f_c}\right|_0$ = 1.315e+02 $\left.\frac{\partial \dot{Q}_e}{\partial f_c}\right|_0$ = 1.027e+02 $\left.\frac{\partial \dot{Q}_e}{\partial dT_c}\right|_0$ = 2.235e+01

$\left.\frac{\partial \dot{W}_c}{\partial dT_e}\right|_0$ = 1.587e+00 $\left.\frac{\partial \dot{Q}_c}{\partial T_{eo}}\right|_0$ = 1.884e+02 $\left.\frac{\partial \dot{Q}_e}{\partial T_{eo}}\right|_0$ = 1.824e+02

$\left.\frac{\partial \dot{W}_c}{\partial T_{co}}\right|_0$ = 3.859e+01 $\left.\frac{\partial \dot{Q}_c}{\partial dT_e}\right|_0$ = 4.119e+01 $\left.\frac{\partial \dot{Q}_e}{\partial dT_e}\right|_0$ = 3.984e+01

Table A.1
Winter Ground: Polynomial models adjusted with the virtual database.

	$\dot{W}_c/f_c$ (W/Hz)	$\dot{Q}_c/f_c$ (W/Hz)	$\dot{Q}_e/f_c$ (W/Hz)
$(Int.)$	1.162e+03 (±1.35e+01)***	4.617e+03 (±7.31e+01)***	3.710e+03 (±7.33e+01)***
$(T_{co}{}^2)$	7.612e−03 (±1.00e−04)***	9.011e−03 (±5.43e−04)***	3.644e−03 (±5.45e−04)***
T_{co}	−6.997e+00 (±6.74e−02)***	−1.003e+01 (±3.65e−01)***	−4.674e+00 (±3.66e−01)***
$(T_{eo}{}^2)$	−3.968e−03 (±7.56e−05)***	4.359e−02 (±4.09e−04)***	4.690e−02 (±4.10e−04)***
T_{eo}	−1.214e+00 (±4.83e−02)***	−2.405e+01 (±2.62e−01)***	−2.307e+01 (±2.62e−01)***
dT_c	3.013e+00 (±7.38e−02)***	2.669e−01 (±8.87e−03)***	4.470e−01 (±8.90e−03)***
dT_e	3.174e−02 (±1.74e−03)***	8.238e−01 (±9.44e−03)***	7.968e−01 (±9.47e−03)***
f_c	−1.602e−01 (±1.08e−02)***	2.826e−01 (±5.87e−02)***	3.247e−01 (±5.89e−02)***
$(1/f_c)$	2.991e+02 (±2.53e+00)***	−1.275e+02 (±1.37e+01)***	−2.816e+02 (±1.38e+01)***
$T_{co}\times T_{eo}$	1.089e−02 (±7.90e−05)***	1.278e−02 (±4.27e−04)***	3.737e−03 (±4.29e−04)***
$T_{co}\times dT_c$	−1.029e−02 (±2.32e−04)***		
$T_{eo}\times f_c$	1.125e−03 (±3.95e−05)***	−1.270e−03 (±2.14e−04)***	−1.814e−03 (±2.14e−04)***
Num.Obs.	3125	3125	3125
R2 Adj.	1.000	0.999	0.999
MRE (%)	1.385	1.867	3.204
RMSE (W)	5.524	32.030	31.981
CV_{RMSE} (%)	0.293	0.477	0.596
Range (W)	[890, 3558]	[2415, 13500]	[1531, 11939]

[a] + p < 0.1, * p < 0.05, ** p < 0.01, *** p < 0.001; Confidence interval of 95% for regression coefficients;
[b] Temperatures (K);
[c] Compressor frequency (Hz).

Table A.2
Winter Ground: Experimental readjustment.

	$\dot{W}_c^*$ (W)	$\dot{Q}_c^*$ (W)	$\dot{Q}_e^*$ (W)
$k_0(\dot{W}_{c0}, \dot{Q}_{c0}, \dot{Q}_{e0})$	1.000e+00 (±3.06e−03)***	1.012e+00 (±5.66e−03)***	1.007e+00 (±6.16e−03)***
$k_1(x_1 = f_c)$	9.815e−01 (±1.27e−02)***	9.997e−01 (±3.33e−02)***	9.548e−01 (±3.68e−02)***
$k_2(x_2 = T_{eo})$	1.070e+00 (±1.81e−01)***	1.070e+00 (±4.47e−02)***	1.084e+00 (±3.98e−02)***
$k_3(x_3 = dT_e)$	1.274e+00 (±2.22e+00)	7.679e−01 (±5.68e−01)*	8.376e−01 (±5.06e−01)**
$k_4(x_4 = T_{co})$	1.046e+00 (±3.34e−02)***	7.735e−01 (±2.14e−01)***	9.212e−01 (±1.10e−01)***
$k_5(x_5 = dT_c)$	1.163e+00 (±2.68e−01)***		7.768e−01 (±8.94e−01)+
Num.Obs.	30	30	30
R2 Adj.	1.000	1.000	1.000
MRE (%)	2.131	3.543	3.351
RMSE (W)	13.488	91.488	77.069
CV_{RMSE} (%)	0.720	1.354	1.434
Range (W)	[1292, 2663]	[4293, 9988]	[3233, 8517]

[a] + p < 0.1, * p < 0.05, ** p < 0.01, *** p < 0.001; Confidence interval of 95% for regression coefficients;
[b] Temperatures (K);
[c] Compressor frequency (Hz).

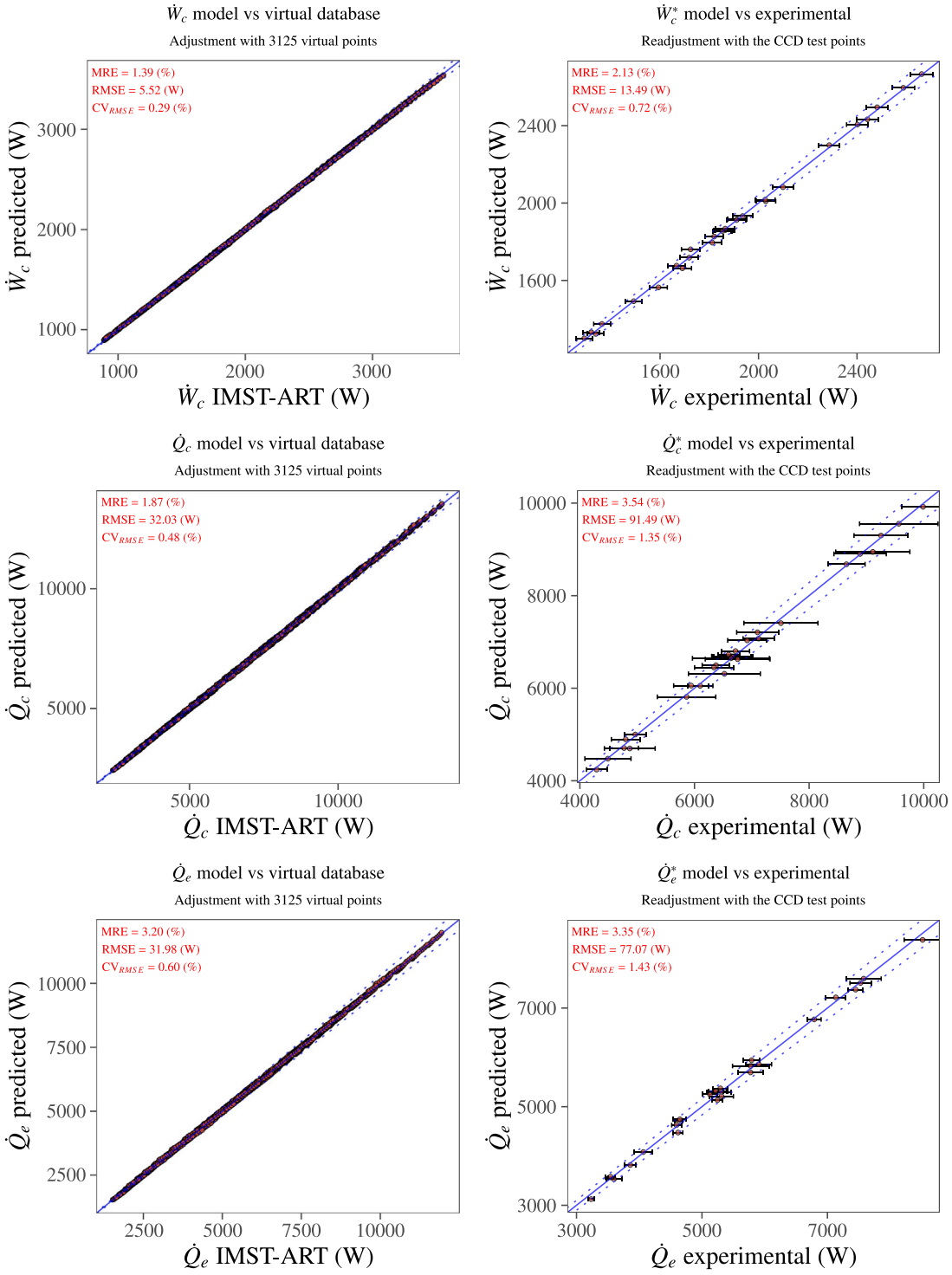

Fig. A.1. Winter Ground mode: Empirical model.

A.2. Summer ground

CCD central point:

$\dot{W}_{c0}$ = 1082.285 (W) $\dot{Q}_{e0}$ = 8880.096 (W) T_{eo0} = 283.59 (K)

$\dot{Q}_{c0}$ = 9998.515 (W) f_{c0} = 50 (Hz) T_{co0} = 294.055 (K)

Partial derivatives at CCD center point:

$\left.\frac{\partial \dot{W}_c}{\partial f_c}\right|_0$ = 2.381e+01 $\left.\frac{\partial \dot{Q}_c}{\partial f_c}\right|_0$ = 1.963e+02 $\left.\frac{\partial \dot{Q}_e}{\partial f_c}\right|_0$ = 1.783e+02

$\left.\frac{\partial \dot{W}_c}{\partial T_{eo}}\right|_0$ = −1.123e+01 $\left.\frac{\partial \dot{Q}_c}{\partial T_{eo}}\right|_0$ = 2.273e+02 $\left.\frac{\partial \dot{Q}_e}{\partial T_{eo}}\right|_0$ = 2.359e+02

$\left.\frac{\partial \dot{W}_c}{\partial T_{co}}\right|_0$ = 2.547e+01 $\left.\frac{\partial \dot{Q}_c}{\partial T_{co}}\right|_0$ = −4.824e+01 $\left.\frac{\partial \dot{Q}_e}{\partial T_{co}}\right|_0$ = −6.648e+01

Table A.3
Summer Ground: Polynomial models adjusted with the virtual database.

	$\dot{W}_c/f_c$ (W/Hz)	$\dot{Q}_c/f_c$ (W/Hz)	$\dot{Q}_e/f_c$ (W/Hz)
($Int.$)	1.267e+03 (±1.82e+01)***	6.361e+03 (±1.92e+02)***	5.469e+03 (±1.94e+02)***
(T_{co}^2)	8.446e−03 (±1.03e−04)***	7.825e−03 (±9.53e−04)***	2.714e−03 (±9.64e−04)***
T_{co}	−7.624e+00 (±5.66e−02)***	−1.115e+01 (±5.41e−01)***	−6.019e+00 (±5.46e−01)***
(T_{eo}^2)	−4.286e−03 (±2.23e−04)***	6.029e−02 (±2.37e−03)***	6.323e−02 (±2.39e−03)***
T_{eo}	−1.186e+00 (±1.19e−01)***	−3.540e+01 (±1.27e+00)***	−3.430e+01 (±1.28e+00)***
dT_c	1.429e+00 (±7.03e−02)***	1.377e−01 (±1.34e−02)***	2.019e−01 (±1.35e−02)***
dT_e	−5.151e−02 (±1.19e−03)***	1.321e+00 (±1.27e−02)***	1.360e+00 (±1.29e−02)***
f_c	−3.521e−01 (±1.52e−02)***		
($1/f_c$)	1.857e+02 (±1.86e+00)***	−4.043e+02 (±1.97e+01)***	−5.444e+02 (±2.00e+01)***
$T_{co}\times T_{eo}$	1.125e−02 (±1.79e−04)***	1.968e−02 (±1.89e−03)***	1.091e−02 (±1.91e−03)***
$T_{co}\times dT_c$	−5.116e−03 (±2.36e−04)***		
$T_{eo}\times f_c$	1.653e−03 (±5.35e−05)***	−6.639e−04 (±3.27e−05)***	−9.717e−04 (±3.31e−05)***
Num.Obs.	2096	2096	2096
R2 Adj.	0.999	0.998	0.998
MRE (%)	1.269	1.141	1.286
RMSE (W)	3.578	38.031	38.663
CV_{RMSE} (%)	0.287	0.373	0.417
Range (W)	[584, 2188]	[4869, 16826]	[4191, 15668]

[a] + p < 0.1, * p < 0.05, ** p < 0.01, *** p < 0.001; Confidence interval of 95% for regression coefficients;
[b] Temperatures (K);
[c] Compressor frequency (Hz).

Table A.4
Summer Ground: Experimental readjustment.

	$\dot{W}_c^*$ (W)	$\dot{Q}_c^*$ (W)	$\dot{Q}_e^*$ (W)
$k_0(\dot{W}_{c0}, \dot{Q}_{c0}, \dot{Q}_{e0})$	9.870e−01 (±1.83e−02)***	1.016e+00 (±2.51e−02)***	9.851e−01 (±2.73e−02)***
$k_1(x_1 = f_c)$	1.107e+00 (±5.63e−02)***	9.696e−01 (±8.64e−02)***	9.110e−01 (±9.17e−02)***
$k_2(x_2 = T_{eo})$	5.389e−01 (±4.05e−01)*	1.149e+00 (±2.53e−01)***	1.087e+00 (±2.35e−01)***
$k_3(x_3 = T_{co})$	1.088e+00 (±1.16e−01)***	8.479e−01 (±7.73e−01)*	8.874e−01 (±5.41e−01)*
Num.Obs.	8	8	8
R2 Adj.	1.000	1.000	1.000
MRE (%)	1.087	2.235	2.122
RMSE (W)	6.612	83.672	80.695
CV_{RMSE} (%)	0.616	0.940	1.029
Range (W)	[577, 1588]	[6622, 11013]	[6021, 9434]

[a] + p < 0.1, * p < 0.05, ** p < 0.01, *** p < 0.001; Confidence interval of 95% for regression coefficients;
[b] Temperatures (K);
[c] Compressor frequency (Hz).

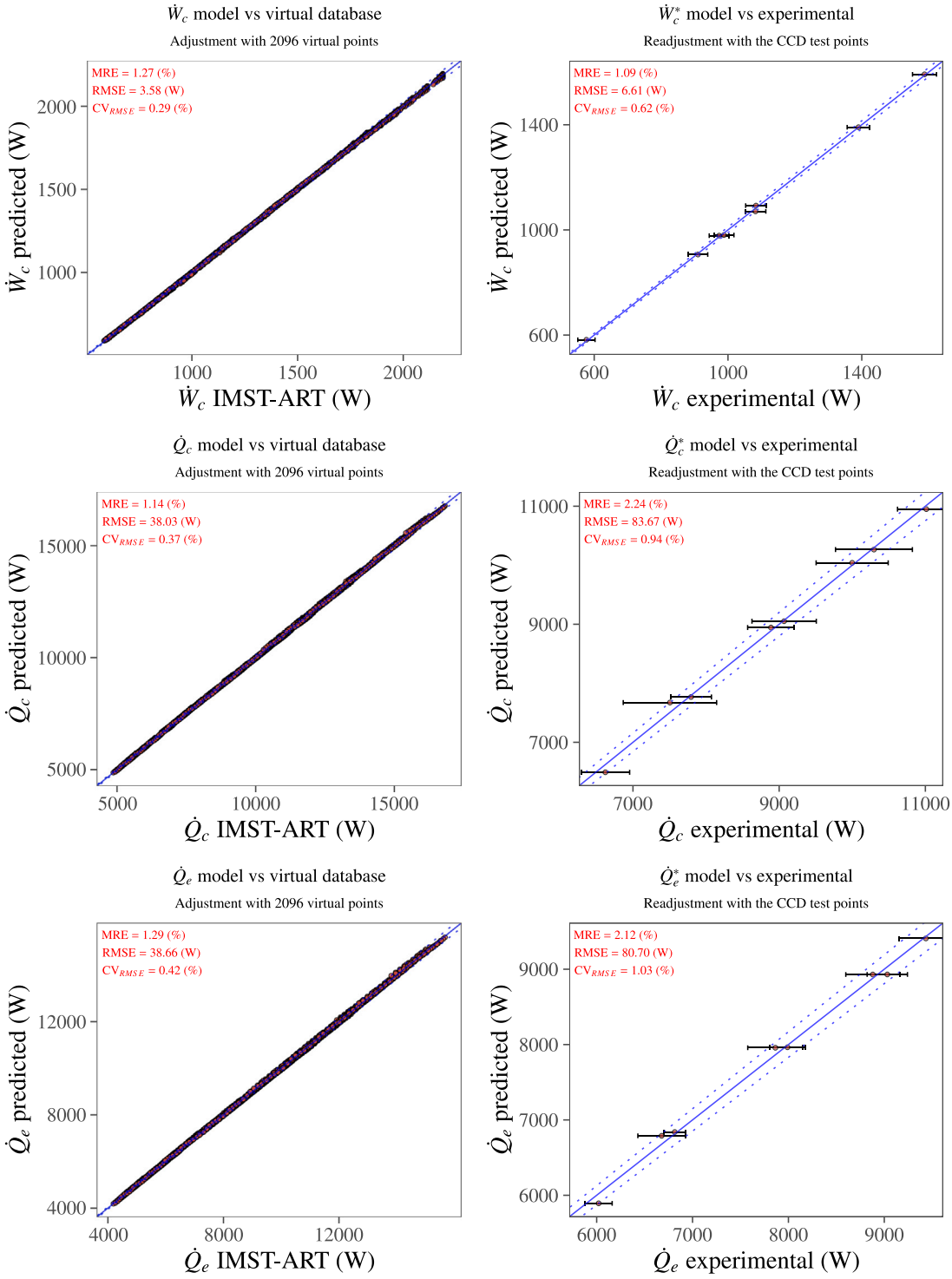

Fig. A.2. Summer Ground mode: Empirical model.

A.3. DHW ground

CCD central point:

$\dot{W}_{c0}$ = 2038.856 (W) $\dot{Q}_{e0}$ = 6012.805 (W) T_{eo0} = 278.163 (K)

$\dot{Q}_{c0}$ = 7315.763 (W) f_{c0} = 50 (Hz) dT_{e0} = 4.974 (K)

dT_{c0} = 20.049 (K)

Partial derivatives at CCD center point:

$\left.\frac{\partial \dot{W}_c}{\partial f_c}\right|_0$ = 4.119e+01 $\left.\frac{\partial \dot{W}_c}{\partial dT_c}\right|_0$ = −1.020e+01 $\left.\frac{\partial \dot{Q}_c}{\partial dT_e}\right|_0$ = 4.829e+01 $\left.\frac{\partial \dot{Q}_e}{\partial dT_e}\right|_0$ = 4.614e+01

$\left.\frac{\partial \dot{W}_c}{\partial T_{eo}}\right|_0$ = 8.459e+00 $\left.\frac{\partial \dot{Q}_c}{\partial f_c}\right|_0$ = 1.498e+02 $\left.\frac{\partial \dot{Q}_c}{\partial f_c}\right|_0$ = 1.184e+02 $\left.\frac{\partial \dot{Q}_e}{\partial dT_c}\right|_0$ = 1.717e+01

$\left.\frac{\partial \dot{W}_c}{\partial dT_e}\right|_0$ = 2.658e+00 $\left.\frac{\partial \dot{Q}_c}{\partial T_{eo}}\right|_0$ = 2.132e+02 $\left.\frac{\partial \dot{Q}_e}{\partial T_{eo}}\right|_0$ = 2.063e+02

Table A.5
DHW Ground: Polynomial models adjusted with the virtual database.

	$\dot{W}_c/f_c$ (W/Hz)	$\dot{Q}_c/f_c$ (W/Hz)	$\dot{Q}_e/f_c$ (W/Hz)
(*Int.*)	9.213e+02 (±6.27e+01)***	2.666e+03 (±8.42e+01)***	2.276e+03 (±9.37e+01)***
(T_{co}^2)	4.745e−03 (±5.66e−04)***		
T_{co}	−5.277e+00 (±3.74e−01)***	−9.170e−01 (±2.46e−01)***	1.116e+00 (±2.73e−01)***
(T_{eo}^2)	−3.769e−03 (±5.44e−05)***	4.408e−02 (±3.13e−04)***	4.739e−02 (±3.49e−04)***
T_{eo}	−1.485e+00 (±5.88e−02)***	−2.056e+01 (±3.38e−01)***	−1.948e+01 (±3.76e−01)***
(dT_c^2)	2.853e−03 (±4.77e−05)***		
dT_c	2.271e+00 (±4.30e−02)***	1.839e−01 (±2.66e−03)***	3.434e−01 (±2.96e−03)***
dT_e	5.316e−02 (±2.38e−03)***	9.658e−01 (±1.37e−02)***	9.227e−01 (±1.52e−02)***
f_c	−2.510e−01 (±1.08e−02)***		
$(1/f_c)$	3.284e+02 (±3.57e+00)***	−1.533e+02 (±2.03e+01)***	−3.142e+02 (±2.26e+01)***
$T_{co}\times T_{eo}$	1.137e−02 (±1.53e−04)***	9.794e−04 (±8.84e−04)*	−8.406e−03 (±9.83e−04)***
$T_{co}\times dT_c$	−8.011e−03 (±1.31e−04)***		
$T_{eo}\times f_c$	1.522e−03 (±3.84e−05)***	−2.976e−04 (±3.50e−05)***	−7.576e−04 (±3.89e−05)***
Num.Obs.	3125	3125	3125
R2 Adj.	0.999	1.000	0.999
MRE (%)	1.506	4.259	7.834
RMSE (W)	8.963	50.027	56.302
CV_{RMSE} (%)	0.411	0.658	0.929
Range (W)	[999, 4107]	[2313, 16783]	[1391, 14773]

[a] + p < 0.1, * p < 0.05, ** p < 0.01, *** p < 0.001; Confidence interval of 95% for regression coefficients;
[b] Temperatures (K);
[c] Compressor frequency (Hz).

Table A.6
DHW Ground: Experimental readjustment.

	$\dot{W}_c^*$ (W)	$\dot{Q}_c^*$ (W)	$\dot{Q}_e^*$ (W)
$k_0(\dot{W}_{c0}, \dot{Q}_{c0}, \dot{Q}_{e0})$	1.033e+00 (±5.11e−03)***	9.714e−01 (±9.38e−03)***	9.886e−01 (±5.94e−03)***
$k_1(x_1 = f_c)$	1.007e+00 (±3.00e−02)***	9.586e−01 (±5.42e−02)***	9.122e−01 (±3.57e−02)***
$k_2(x_2 = T_{eo})$	1.197e+00 (±1.83e−01)***	1.031e+00 (±4.79e−02)***	1.047e+00 (±2.57e−02)***
$k_3(x_3 = dT_e)$	3.517e−01 (±2.45e+00)	9.280e−01 (±8.88e−01)*	1.041e+00 (±4.83e−01)***
$k_4(x_4 = dT_c)$	9.181e−01 (±1.21e−01)***		7.931e−01 (±2.46e−01)***
Num.Obs.	20	20	20
R2 Adj.	1.000	1.000	1.000
MRE (%)	1.756	4.721	2.100
RMSE (W)	18.918	129.369	64.792
CV_{RMSE} (%)	0.927	1.732	1.046
Range (W)	[1451, 2910]	[4436, 11425]	[3437, 10005]

[a] + p < 0.1, * p < 0.05, ** p < 0.01, *** p < 0.001; Confidence interval of 95% for regression coefficients;
[b] Temperatures (K);
[c] Compressor frequency (Hz).

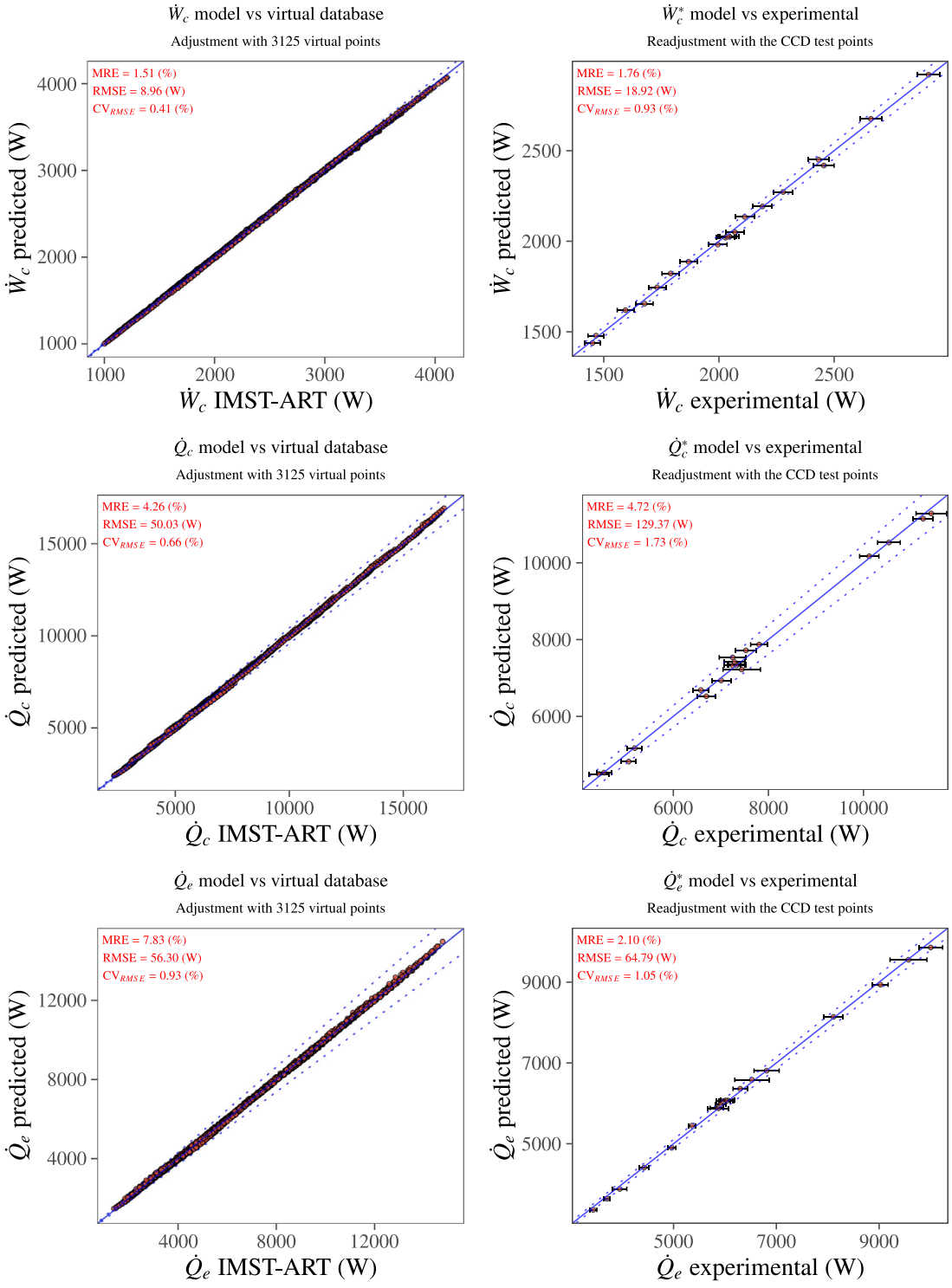

Fig. A.3. DHW Ground mode: Empirical model.

A.4. DHW user

CCD central point:

$\dot{W}_{c0}$ = 2083.81 (W) $\dot{Q}_{e0}$ = 7575.931 (W) T_{eo0} = 285.111 (K)

$\dot{Q}_{c0}$ = 9296.505 (W) f_{c0} = 50 (Hz) dT_{e0} = 5.031 (K)

dT_{c0} = 20.021 (K)

Partial derivatives at CCD center point:

$\left.\frac{\partial \dot{W}_c}{\partial f_c}\right|_0$ = 4.281e+01 $\left.\frac{\partial \dot{W}_c}{\partial dT_c}\right|_0$ = −1.063e+01 $\left.\frac{\partial \dot{Q}_c}{\partial dT_e}\right|_0$ = 7.123e+01 $\left.\frac{\partial \dot{Q}_e}{\partial dT_e}\right|_0$ = 6.935e+01

$\left.\frac{\partial \dot{W}_c}{\partial T_{eo}}\right|_0$ = 5.470e+00 $\left.\frac{\partial \dot{Q}_c}{\partial f_c}\right|_0$ = 1.848e+02 $\left.\frac{\partial \dot{Q}_e}{\partial f_c}\right|_0$ = 1.522e+02 $\left.\frac{\partial \dot{Q}_e}{\partial dT_c}\right|_0$ = 1.651e+01

$\left.\frac{\partial \dot{W}_c}{\partial dT_e}\right|_0$ = 2.350e+00 $\left.\frac{\partial \dot{Q}_c}{\partial T_{eo}}\right|_0$ = 2.503e+02 $\left.\frac{\partial \dot{Q}_e}{\partial T_{eo}}\right|_0$ = 2.459e+02

Table A.7
DHW User: Polynomial models adjusted with the virtual database.

	$\dot{W}_c/f_c$ (W/Hz)	$\dot{Q}_c/f_c$ (W/Hz)	$\dot{Q}_e/f_c$ (W/Hz)
(*Int.*)	8.516e+02 (±6.26e+01)***	2.085e+03 (±2.36e+02)***	1.767e+03 (±2.85e+02)***
(T_{co}^2)	4.540e−03 (±4.54e−04)***		
T_{co}	−5.095e+00 (±3.11e−01)***	1.393e+00 (±5.44e−01)***	3.245e+00 (±6.56e−01)***
(T_{eo}^2)	−4.236e−03 (±3.15e−04)***	4.654e−02 (±1.90e−03)***	5.003e−02 (±2.29e−03)***
T_{eo}	−1.188e+00 (±2.08e−01)***	−1.923e+01 (±1.25e+00)***	−1.845e+01 (±1.51e+00)***
(dT_c^2)	2.879e−03 (±3.83e−05)***		
dT_c	2.183e+00 (±3.44e−02)***	1.604e−01 (±2.23e−03)***	3.302e−01 (±2.69e−03)***
dT_e	4.699e−02 (±1.85e−03)***	1.425e+00 (±1.12e−02)***	1.387e+00 (±1.35e−02)***
f_c	−3.203e−01 (±2.26e−02)***		
$(1/f_c)$	3.372e+02 (±2.86e+00)***	−1.982e+02 (±1.72e+01)***	−4.137e+02 (±2.08e+01)***
$T_{co}\times T_{eo}$	1.121e−02 (±3.16e−04)***	−7.054e−03 (±1.91e−03)***	−1.585e−02 (±2.30e−03)***
$T_{co}\times dT_c$	−7.767e−03 (±1.05e−04)***		
$T_{eo}\times f_c$	1.786e−03 (±7.91e−05)***	−3.569e−04 (±2.89e−05)***	−8.473e−04 (±3.49e−05)***
Num.Obs.	3125	3125	3125
R2 Adj.	0.999	0.999	0.998
MRE (%)	1.150	1.458	2.587
RMSE (W)	7.123	39.704	49.260
CV_{RMSE} (%)	0.313	0.432	0.655
Range (W)	[1104, 4072]	[4297, 15772]	[3145, 13731]

[a] + p < 0.1, * p < 0.05, ** p < 0.01, *** p < 0.001; Confidence interval of 95% for regression coefficients;
[b] Temperatures (K);
[c] Compressor frequency (Hz).

Table A.8
DHW User: Experimental readjustment.

	$\dot{W}_c^*$ (W)	$\dot{Q}_c^*$ (W)	$\dot{Q}_e^*$ (W)
$k_0(\dot{W}_{c0}, \dot{Q}_{c0}, \dot{Q}_{e0})$	1.032e+00 (±4.05e−03)***	9.968e−01 (±6.40e−03)***	9.660e−01 (±4.09e−03)***
$k_1(x_1 = f_c)$	1.029e+00 (±2.20e−02)***	1.021e+00 (±3.59e−02)***	9.548e−01 (±2.27e−02)***
$k_2(x_2 = T_{eo})$	8.159e−01 (±5.83e−01)**	1.031e+00 (±8.98e−02)***	1.031e+00 (±4.76e−02)***
$k_3(x_3 = dT_e)$	4.703e−01 (±2.29e+00)	1.226e+00 (±5.32e−01)***	1.324e+00 (±2.84e−01)***
$k_4(x_4 = dT_c)$	8.079e−01 (±9.38e−02)***		8.725e−01 (±2.22e−01)***
Num.Obs.	20	20	20
R2 Adj.	1.000	1.000	1.000
MRE (%)	1.505	2.776	1.672
RMSE (W)	15.290	111.968	56.137
CV_{RMSE} (%)	0.730	1.208	0.745
Range (W)	[1261, 3011]	[5515, 12998]	[4596, 10401]

[a] + p < 0.1, * p < 0.05, ** p < 0.01, *** p < 0.001; Confidence interval of 95% for regression coefficients;
[b] Temperatures (K);
[c] Compressor frequency (Hz).

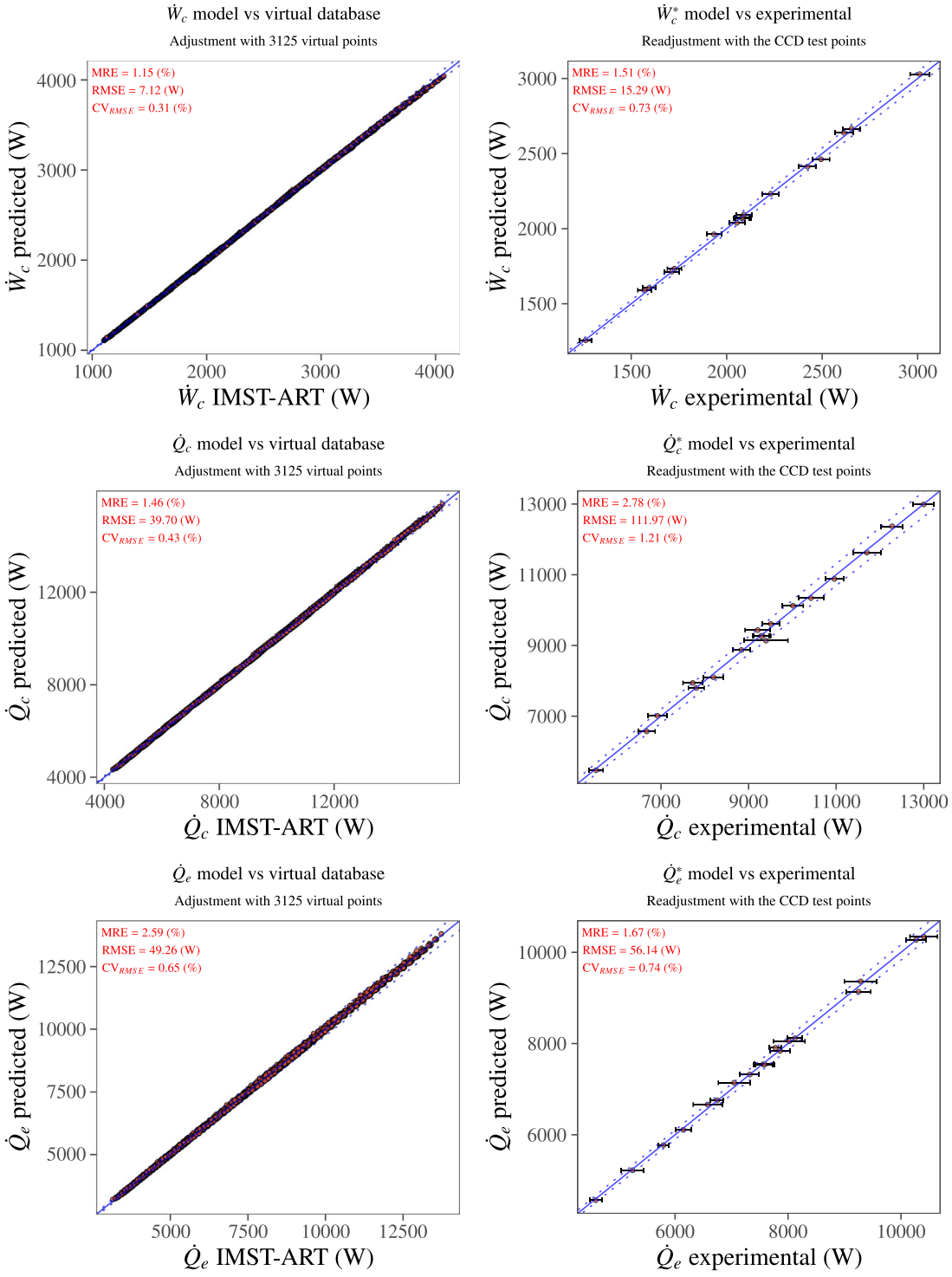

Fig. A.4. DHW User mode: Empirical model.

A.5. Winter air

CCD central point:

$\dot{W}_{c0}$ = 1897.929 (W) f_{c0} = 50 (Hz) T_{co0} = 318.163 (K)

$\dot{Q}_{c0}$ = 7845.713 (W) T_{ei0} = 284.156 (K) dT_{c0} = 4.994 (K)

$\dot{Q}_{e0}$ = 6646.5 (W) f_{fan0} = 50 (%) $\Delta w'_0$ = 0.00181 ($kg_{water}/kg_{dry\ air}$)

Partial derivatives at CCD center point:

$\left.\frac{\partial \dot{W}_c}{\partial f_c}\right|_0$ = 3.979e+01 $\left.\frac{\partial \dot{W}_c}{\partial dT_c}\right|_0$ = −1.362e+01 $\left.\frac{\partial \dot{Q}_c}{\partial T_{co}}\right|_0$ = −3.341e+01 $\left.\frac{\partial \dot{Q}_e}{\partial f_{fan}}\right|_0$ = 8.002e+00

$\left.\frac{\partial \dot{W}_c}{\partial T_{ei}}\right|_0$ = 3.092e+00 $\left.\frac{\partial \dot{Q}_c}{\partial f_c}\right|_0$ = 1.643e+02 $\left.\frac{\partial \dot{Q}_c}{\partial \Delta w'}\right|_0$ = 1.167e+05 $\left.\frac{\partial \dot{Q}_e}{\partial T_{co}}\right|_0$ = −6.374e+01

$\left.\frac{\partial \dot{W}_c}{\partial f_{fan}}\right|_0$ = 6.673e-02 $\left.\frac{\partial \dot{Q}_c}{\partial T_{ei}}\right|_0$ = 1.990e+02 $\left.\frac{\partial \dot{Q}_e}{\partial f_c}\right|_0$ = 1.343e+02 $\left.\frac{\partial \dot{Q}_e}{\partial \Delta w'}\right|_0$ = 1.105e+05

$\left.\frac{\partial \dot{W}_c}{\partial T_{co}}\right|_0$ = 4.294e+01 $\left.\frac{\partial \dot{Q}_c}{\partial f_{fan}}\right|_0$ = 8.081e+00 $\left.\frac{\partial \dot{Q}_e}{\partial T_{ei}}\right|_0$ = 1.959e+02

Table A.9
Winter Air: Polynomial models adjusted with the virtual database.

	$\dot{W}_c/f_c$ (W/Hz)	$\dot{Q}_c/f_c$ (W/Hz)	$\dot{Q}_e/f_c$ (W/Hz)
(*Int.*)	1.022e+03 (±2.73e+01)***	−1.255e+03 (±1.62e+01)***	−1.073e+03 (±1.45e+01)***
(T_{co}^2)	7.564e−03 (±1.33e−04)***		
T_{co}	−6.643e+00 (±9.46e−02)***	−6.682e−01 (±6.64e−03)***	−1.275e+00 (±5.94e−03)***
(T_{ei}^2)	−4.325e−03 (±2.42e−04)***		
T_{ei}	−6.008e−01 (±1.45e−01)***	5.833e+00 (±5.57e−02)***	5.806e+00 (±4.98e−02)***
dT_c	2.873e+00 (±9.81e−02)***	2.098e−01 (±1.83e−02)***	4.023e−01 (±1.64e−02)***
$(1/f_{fan})$	−3.337e+00 (±9.72e−01)***	1.347e+04 (±4.31e+02)***	1.348e+04 (±3.85e+02)***
f_c	−1.608e−01 (±2.16e−02)***	4.969e+00 (±2.60e−01)***	5.044e+00 (±2.32e−01)***
$(1/f_c)$	2.969e+02 (±3.41e+00)***	−4.158e+02 (±2.93e+01)***	−5.731e+02 (±2.62e+01)***
$T_{co}\times T_{ei}$	9.634e−03 (±1.47e−04)***		
$T_{co}\times dT_c$	−9.887e−03 (±3.08e−04)***		
$T_{ei}\times f_c$	1.113e−03 (±7.56e−05)***	−1.825e−02 (±8.97e−04)***	−1.893e−02 (±8.03e−04)***
$\Delta w'$		−2.626e+03 (±3.43e+02)***	−2.723e+03 (±3.07e+02)***
$\Delta w'\times f_c$		9.920e+01 (±6.75e+00)***	9.865e+01 (±6.04e+00)***
$T_{ei}\times(1/f_{fan})$		−4.701e+01 (±1.51e+00)***	−4.707e+01 (±1.35e+00)***
$(1/f_{fan})\times f_c$		−1.027e+01 (±6.64e−01)***	−1.003e+01 (±5.94e−01)***
Num.Obs.	2375	2375	2375
R2 Adj.	0.999	0.997	0.998
MRE (%)	1.806	2.465	2.891
RMSE (W)	6.319	58.656	51.994
CV_{RMSE} (%)	0.333	0.720	0.766
Range (W)	[872, 3586]	[3826, 14063]	[2829, 12507]

[a] + p < 0.1, * p < 0.05, ** p < 0.01, *** p < 0.001; Confidence interval of 95% for regression coefficients;
[b] Temperatures (K);
[c] Compressor frequency (Hz);
[d] Fan frequency (%);
[e] $\Delta w'$ ($kg_{water}/kg_{dry\ air}$);
[f] δT_e = 6 K.

Table A.10
Winter Air: Experimental readjustment.

	$\dot{W}_c^*$ (W)	$\dot{Q}_c^*$ (W)	$\dot{Q}_e^*$ (W)
$k_0(\dot{W}_{c0},\ \dot{Q}_{c0},\ \dot{Q}_{e0})$	9.985e−01 (±2.68e−03)***	9.244e−01 (±7.08e−03)***	9.336e−01 (±8.27e−03)***
$k_1(x_1 = f_c)$	9.924e−01 (±1.42e−02)***	9.118e−01 (±2.41e−02)***	9.120e−01 (±2.92e−02)***
$k_2(x_2 = T_{ei})$	1.024e+00 (±4.67e−01)***	9.588e−01 (±6.59e−02)***	1.020e+00 (±6.63e−02)***
$k_3(x_3 = f_{fan})$	5.713e+00 (±5.65e+00)*	1.395e+00 (±3.27e−01)***	1.603e+00 (±3.27e−01)***
$k_4(x_4 = T_{co})$	9.852e−01 (±2.65e−02)***	8.280e−01 (±2.39e−01)***	9.077e−01 (±1.24e−01)***
$k_5(x_5 = dT_c)$	1.107e+00 (±2.35e−01)***		
$k_6(x_6 = \Delta w')$		1.066e+00 (±5.93e−01)**	1.826e+00 (±6.21e−01)***
Num.Obs.	30	30	30
R2 Adj.	1.000	1.000	1.000
MRE (%)	1.966	2.783	3.325
RMSE (W)	12.000	84.117	83.303
CV_{RMSE} (%)	0.629	1.095	1.302
Range (W)	[1176, 2740]	[4763, 10699]	[3945, 8828]

[a] + p < 0.1, * p < 0.05, ** p < 0.01, *** p < 0.001; Confidence interval of 95% for regression coefficients;
[b] Temperatures (K);
[c] Compressor frequency (Hz);
[d] Fan frequency (%);
[e] $\Delta w'$ ($kg_{water}/kg_{dry\ air}$);
[f] δT_e = 6 K.

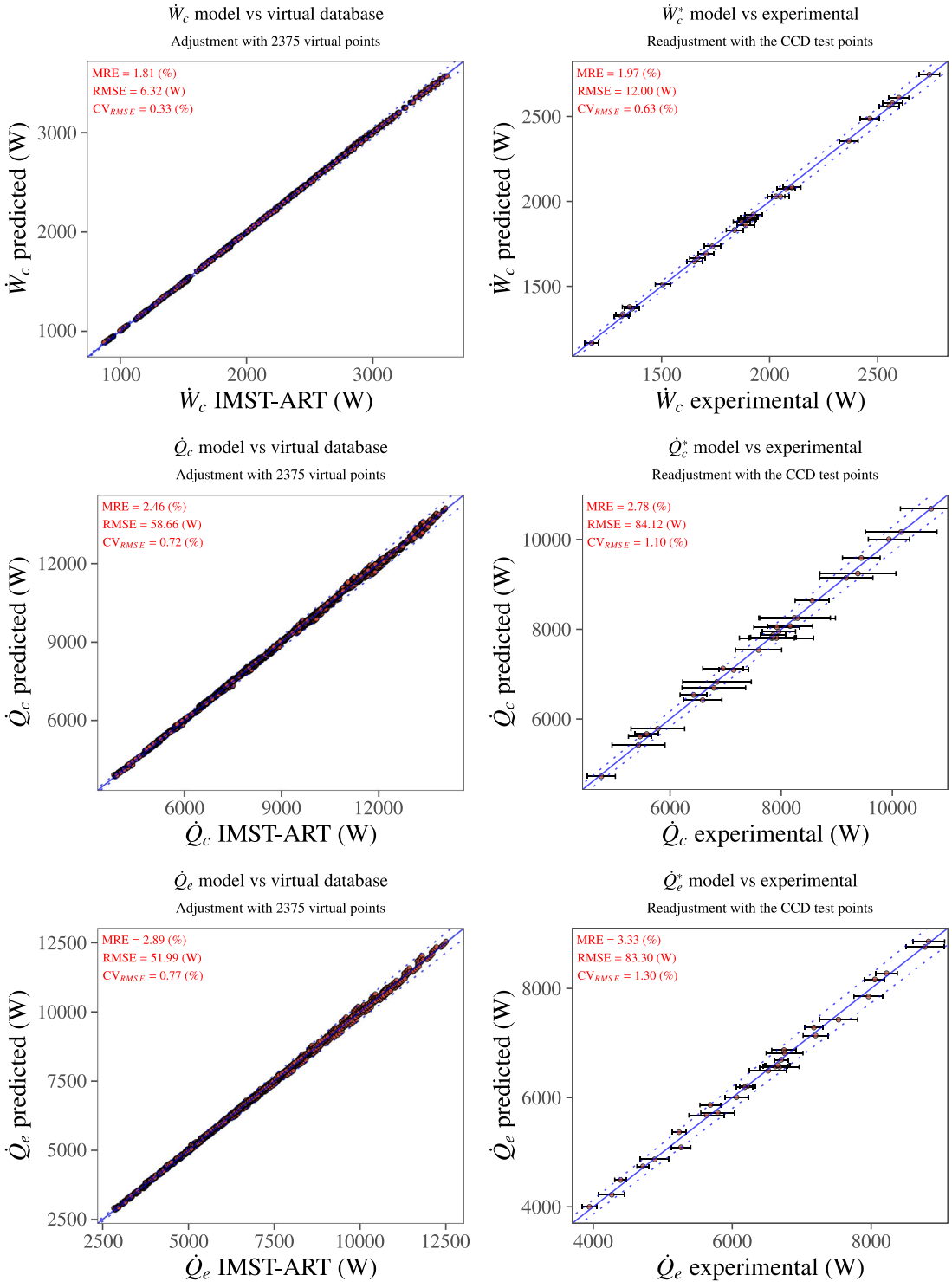

Fig. A.5. Winter Air mode: Empirical model.

A.6. Summer air

CCD central point:

$\dot{W}_{c0}$ = 1590.636 (W) $\dot{Q}_{e0}$ = 8378.182 (W) T_{ci0} = 300.153 (K)

T_{eo0} = 285.163 (K) $\dot{Q}_{c0}$ = 9383 (W) f_{c0} = 50 (Hz)

f_{fan0} = 50 (%) dT_{e0} = 4.962 (K)

Partial derivatives at CCD center point:

$\left.\frac{\partial \dot{W}_c}{\partial f_c}\right|_0$ = 3.849e+01 $\left.\frac{\partial \dot{Q}_c}{\partial f_c}\right|_0$ = 1.895e+02 $\left.\frac{\partial \dot{Q}_c}{\partial dT_e}\right|_0$ = 7.344e+01 $\left.\frac{\partial \dot{Q}_e}{\partial T_{eo}}\right|_0$ = 2.386e+02

$\left.\frac{\partial \dot{W}_c}{\partial T_{ci}}\right|_0$ = 3.834e+01 $\left.\frac{\partial \dot{Q}_c}{\partial T_{ci}}\right|_0$ = −3.932e+01 $\left.\frac{\partial \dot{Q}_e}{\partial f_c}\right|_0$ = 1.608e+02 $\left.\frac{\partial \dot{Q}_e}{\partial dT_e}\right|_0$ = 7.290e+01

$\left.\frac{\partial \dot{W}_c}{\partial f_{fan}}\right|_0$ = −4.446e+00 $\left.\frac{\partial \dot{Q}_c}{\partial f_{fan}}\right|_0$ = 4.234e+00 $\left.\frac{\partial \dot{Q}_e}{\partial T_{ci}}\right|_0$ = −6.670e+01

$\left.\frac{\partial \dot{W}_c}{\partial T_{eo}}\right|_0$ = 3.230e+00 $\left.\frac{\partial \dot{Q}_c}{\partial T_{eo}}\right|_0$ = 2.409e+02 $\left.\frac{\partial \dot{Q}_e}{\partial f_{fan}}\right|_0$ = 7.245e+00

Table A.11
Summer Air: Polynomial models adjusted with the virtual database.

	$\dot{W}_c/f_c$ (W/Hz)	$\dot{Q}_c/f_c$ (W/Hz)	$\dot{Q}_e/f_c$ (W/Hz)
(*Int.*)	1.946e+03 (±1.93e+01)***	3.700e+03 (±1.62e+02)***	3.787e+03 (±1.57e+02)***
T_{ci}	−8.491e+00 (±8.54e−02)***	−7.865e−01 (±3.62e−03)***	−1.334e+00 (±3.49e−03)***
T_{eo}	−4.827e+00 (±6.11e−02)***	−2.765e+01 (±1.14e+00)***	−2.750e+01 (±1.10e+00)***
dT_e	1.591e−02 (±2.65e−03)***	−7.937e+00 (±7.96e−01)***	−7.889e+00 (±7.68e−01)***
$(1/f_{fan})$	−3.872e+03 (±8.83e+01)***	6.246e+02 (±3.51e+02)***	2.578e+03 (±3.39e+02)***
f_c	−2.067e+00 (±3.76e−02)***	4.075e−01 (±1.51e−01)***	1.572e+00 (±1.46e−01)***
$(T_{ci}{}^2)$	8.178e−03 (±1.15e−04)***		
$(1/f_c)$	2.261e+02 (±4.28e+00)***	−2.868e+02 (±1.85e+01)***	−4.170e+02 (±1.78e+01)***
$T_{ci}\times T_{eo}$	1.467e−02 (±1.98e−04)***		
$T_{ci}\times(1/f_{fan})$	4.046e+00 (±1.42e−01)***		
$T_{ci}\times f_c$	1.673e−03 (±6.18e−05)***		
$T_{eo}\times(1/f_{fan})$	9.272e+00 (±2.80e−01)***	−2.933e+00 (±1.23e+00)***	−1.031e+01 (±1.19e+00)***
$T_{eo}\times f_c$	6.031e−03 (±1.21e−04)***	−2.277e−03 (±5.29e−04)***	−6.927e−03 (±5.10e−04)***
$(1/f_{fan})\times f_c$	4.707e+00 (±9.67e−02)***		
$(T_{eo}{}^2)$		5.691e−02 (±2.00e−03)***	5.724e−02 (±1.93e−03)***
$(dT_e{}^2)$		−9.823e−02 (±6.05e−03)***	−9.787e−02 (±5.84e−03)***
$T_{eo}\times dT_e$		3.640e−02 (±2.78e−03)***	3.618e−02 (±2.68e−03)***
Num.Obs.	2297	2297	2297
R2 Adj.	0.999	0.999	0.999
MRE (%)	3.355	1.477	1.894
RMSE (W)	8.381	36.179	35.344
CV_{RMSE} (%)	0.534	0.375	0.417
Range (W)	[611, 3356]	[4613, 16780]	[3757, 15563]

[a] + p < 0.1, * p < 0.05, ** p < 0.01, *** p < 0.001; Confidence interval of 95% for regression coefficients;
[b] Temperatures (K);
[c] Compressor frequency (Hz);
[d] Fan frequency (%).

Table A.12
Summer Air: Experimental readjustment.

	$\dot{W}_c^*$ (W)	$\dot{Q}_c^*$ (W)	$\dot{Q}_e^*$ (W)
$k_0(\dot{W}_{c0}, \dot{Q}_{c0}, \dot{Q}_{e0})$	1.043e+00 (±2.95e−03)***	9.646e−01 (±4.28e−03)***	9.684e−01 (±3.58e−03)***
$k_1(x_1 = f_c)$	1.054e+00 (±1.38e−02)***	9.142e−01 (±2.38e−02)***	9.104e−01 (±2.09e−02)***
$k_2(x_2 = T_{ci})$	1.036e+00 (±2.42e−02)***	1.323e+00 (±2.01e−01)***	1.205e+00 (±8.84e−02)***
$k_3(x_3 = f_{fan})$	1.135e+00 (±7.80e−02)***	1.660e+00 (±6.97e−01)***	1.478e+00 (±3.04e−01)***
$k_4(x_4 = T_{eo})$	1.977e+00 (±5.48e−01)***	1.138e+00 (±6.25e−02)***	1.108e+00 (±4.71e−02)***
$k_5(x_5 = dT_e)$		1.439e+00 (±3.41e−01)***	1.357e+00 (±2.56e−01)***
Num.Obs.	28	28	28
R2 Adj.	1.000	1.000	1.000
MRE (%)	1.225	2.791	2.399
RMSE (W)	10.685	88.533	66.111
CV_{RMSE} (%)	0.652	0.963	0.818
Range (W)	[883, 2531]	[5933, 12904]	[5282, 11154]

[a] + p < 0.1, * p < 0.05, ** p < 0.01, *** p < 0.001; Confidence interval of 95% for regression coefficients;
[b] Temperatures (K);
[c] Compressor frequency (Hz);
[d] Fan frequency (%).

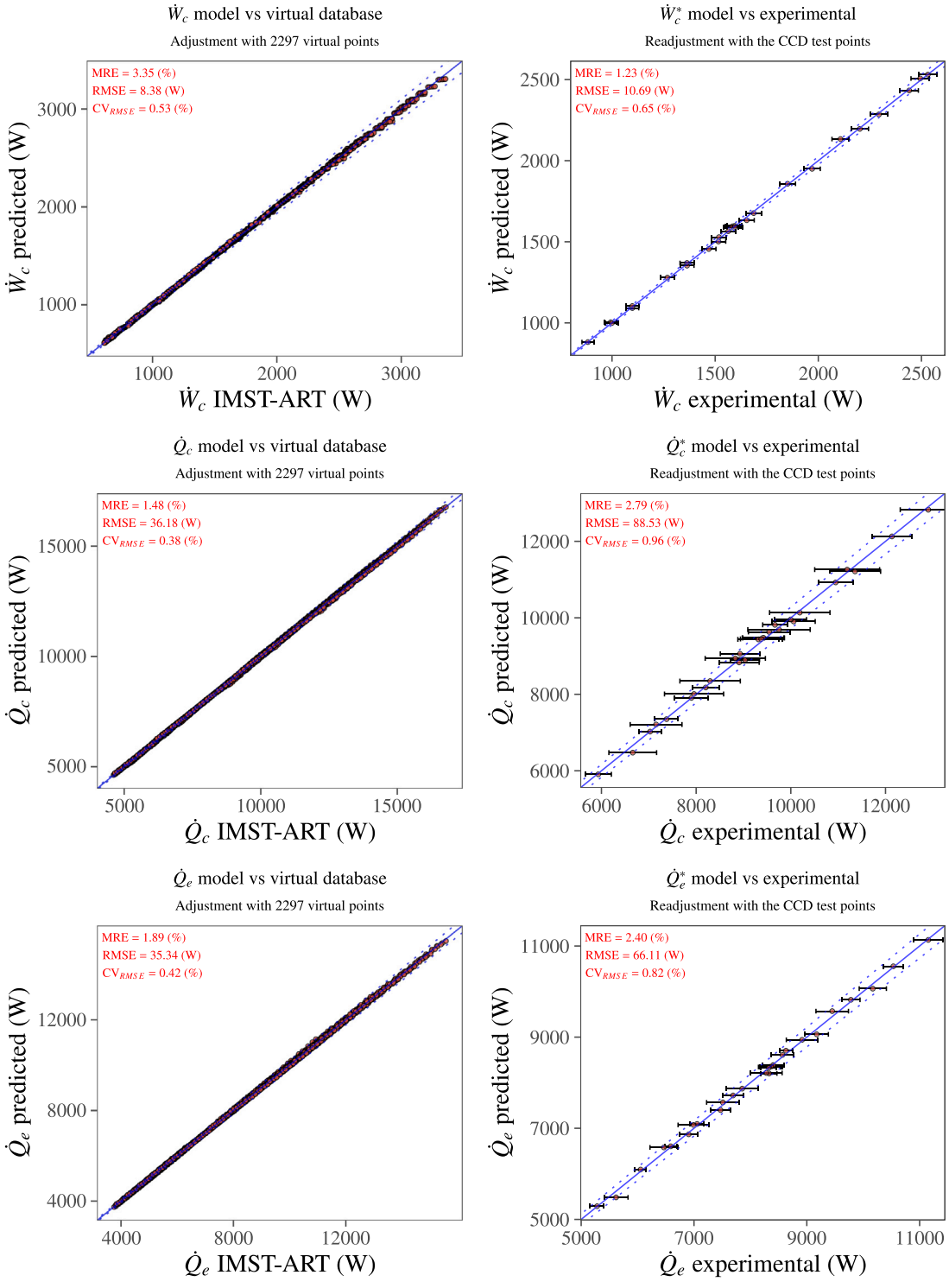

Fig. A.6. Summer Air mode: Empirical model.

A.7. DHW air

CCD central point:

$\dot{W}_{c0}$ = 2076.81 (W) f_{c0} = 50 (Hz) dT_{c0} = 20.02 (K)

$\dot{Q}_{c0}$ = 8407.775 (W) T_{ei0} = 290.07 (K) $\Delta w'_0 = 0$[1] ($kg_{water}/kg_{dry\ air}$)

$\dot{Q}_{e0}$ = 7143.75 (W) f_{fan0} = 50 (%)

[1] There are no dehumidification conditions at the center point.

Partial derivatives at CCD center point:

$\left.\frac{\partial \dot{W}_c}{\partial f_c}\right|_0$ = 4.252e+01 $\left.\frac{\partial \dot{W}_c}{\partial dT_c}\right|_0$ = −1.047e+01 $\left.\frac{\partial \dot{Q}_c}{\partial f_{fan}}\right|_0$ = 1.383e+01 $\left.\frac{\partial \dot{Q}_e}{\partial T_{ei}}\right|_0$ = 2.100e+02

$\left.\frac{\partial \dot{W}_c}{\partial T_{ei}}\right|_0$ = 4.250e+00 $\left.\frac{\partial \dot{Q}_c}{\partial f_c}\right|_0$ = 1.696e+02 $\left.\frac{\partial \dot{Q}_c}{\partial \Delta w'}\right|_0$ = 1.191e+05 $\left.\frac{\partial \dot{Q}_e}{\partial f_{fan}}\right|_0$ = 1.355e+01

$\left.\frac{\partial \dot{W}_c}{\partial f_{fan}}\right|_0$ = 2.998e-01 $\left.\frac{\partial \dot{Q}_c}{\partial T_{ei}}\right|_0$ = 2.158e+02 $\left.\frac{\partial \dot{Q}_e}{\partial f_c}\right|_0$ = 1.374e+02 $\left.\frac{\partial \dot{Q}_e}{\partial \Delta w'}\right|_0$ = 1.144e+05

Table A.13
DHW Air: Polynomial models adjusted with the virtual database.

	$\dot{W}_c/f_c$ (W/Hz)	$\dot{Q}_c/f_c$ (W/Hz)	$\dot{Q}_e/f_c$ (W/Hz)
(*Int.*)	2.732e+02 (±2.61e+01)***	1.109e+02 (±6.77e+01)**	5.899e+02 (±7.20e+01)***
f_c	−1.592e−01 (±1.89e−02)***	7.975e+00 (±1.20e−01)***	8.021e+00 (±1.28e−01)***
T_{co}	−1.708e+00 (±7.29e−02)***	−5.437e−01 (±1.34e−02)***	−1.198e+00 (±1.42e−02)***
T_{ei}	−1.011e+00 (±1.10e−01)***	−4.837e+00 (±4.62e−01)***	−6.745e+00 (±4.92e−01)***
dT_c	2.191e+00 (±5.46e−02)***	1.400e−01 (±3.69e−03)***	3.065e−01 (±3.93e−03)***
$(1/f_{fan})$	−1.499e+01 (±1.31e+00)***	1.492e+04 (±2.82e+02)***	1.479e+04 (±3.00e+02)***
(T_{ei}^2)	−3.580e−03 (±1.25e−04)***	1.997e−02 (±7.92e−04)***	2.310e−02 (±8.44e−04)***
(dT_c^2)	2.874e−03 (±6.07e−05)***		
$(1/f_c)$	3.264e+02 (±4.60e+00)***	−3.529e+02 (±2.95e+01)***	−5.114e+02 (±3.14e+01)***
$T_{co}\times T_{ei}$	9.639e−03 (±2.51e−04)***		
$T_{co}\times dT_c$	−7.786e−03 (±1.66e−04)***		
$f_c\times T_{ei}$	1.167e−03 (±6.46e−05)***		
$\Delta w'$		2.382e+03 (±8.25e+01)***	2.288e+03 (±8.78e+01)***
$T_{ei}\times(1/f_{fan})$		−5.134e+01 (±9.64e−01)***	−5.093e+01 (±1.03e+00)***
$T_{ei}\times f_c$		−2.808e−02 (±4.09e−04)***	−2.872e−02 (±4.36e−04)***
$(1/f_{fan})\times f_c$		−1.437e+01 (±6.69e−01)***	−1.380e+01 (±7.12e−01)***
Num.Obs.	2375	2375	2375
R2 Adj.	0.998	0.999	0.999
MRE (%)	1.383	2.648	3.878
RMSE (W)	9.953	57.066	60.869
CV_{RMSE} (%)	0.448	0.626	0.808
Range (W)	[1095, 4120]	[3888, 16922]	[2805, 14910]

[a] + p < 0.1, * p < 0.05, ** p < 0.01, *** p < 0.001; Confidence interval of 95% for regression coefficients;
[b] Temperatures (K);
[c] Compressor frequency (Hz);
[d] Fan frequency (%);
[e] $\Delta w'$ ($kg_{water}/kg_{dry\ air}$);
[f] δT_e = 7 K.

Table A.14
DHW Air: Experimental readjustment.

	$\dot{W}_c^*$ (W)	$\dot{Q}_c^*$ (W)	$\dot{Q}_e^*$ (W)
$k_0(\dot{W}_{c0}, \dot{Q}_{c0}, \dot{Q}_{e0})$	1.028e+00 (±4.92e−03)***	8.940e−01 (±1.21e−02)***	8.921e−01 (±1.72e−02)***
$k_1(x_1 = f_c)$	1.012e+00 (±2.59e−02)***	9.019e−01 (±5.11e−02)***	9.032e−01 (±7.57e−02)***
$k_2(x_2 = T_{ei})$	1.120e+00 (±4.29e−01)***	9.695e−01 (±8.92e−02)***	9.215e−01 (±1.10e−01)***
$k_3(x_3 = f_{fan})$	2.431e+00 (±2.86e+00)+	1.083e+00 (±4.89e−01)***	1.230e+00 (±6.00e−01)***
$k_4(x_4 = dT_c)$	8.466e−01 (±1.12e−01)***		
$k_5(x_5 = \Delta w')$		1.264e+00 (±1.01e+00)*	7.464e−01 (±1.26e+00)
Num.Obs.	19	19	19
R2 Adj.	1.000	1.000	0.999
MRE (%)	1.681	4.378	5.854
RMSE (W)	17.653	138.660	166.491
CV_{RMSE} (%)	0.849	1.641	2.349
Range (W)	[1259, 2969]	[5213, 11529]	[4365, 9872]

[a] + p < 0.1, * p < 0.05, ** p < 0.01, *** p < 0.001; Confidence interval of 95% for regression coefficients;
[b] Temperatures (K);
[c] Compressor frequency (Hz);
[d] Fan frequency (%);
[e] $\Delta w'$ ($kg_{water}/kg_{dry\ air}$);
[f] δT_e = 7 K.

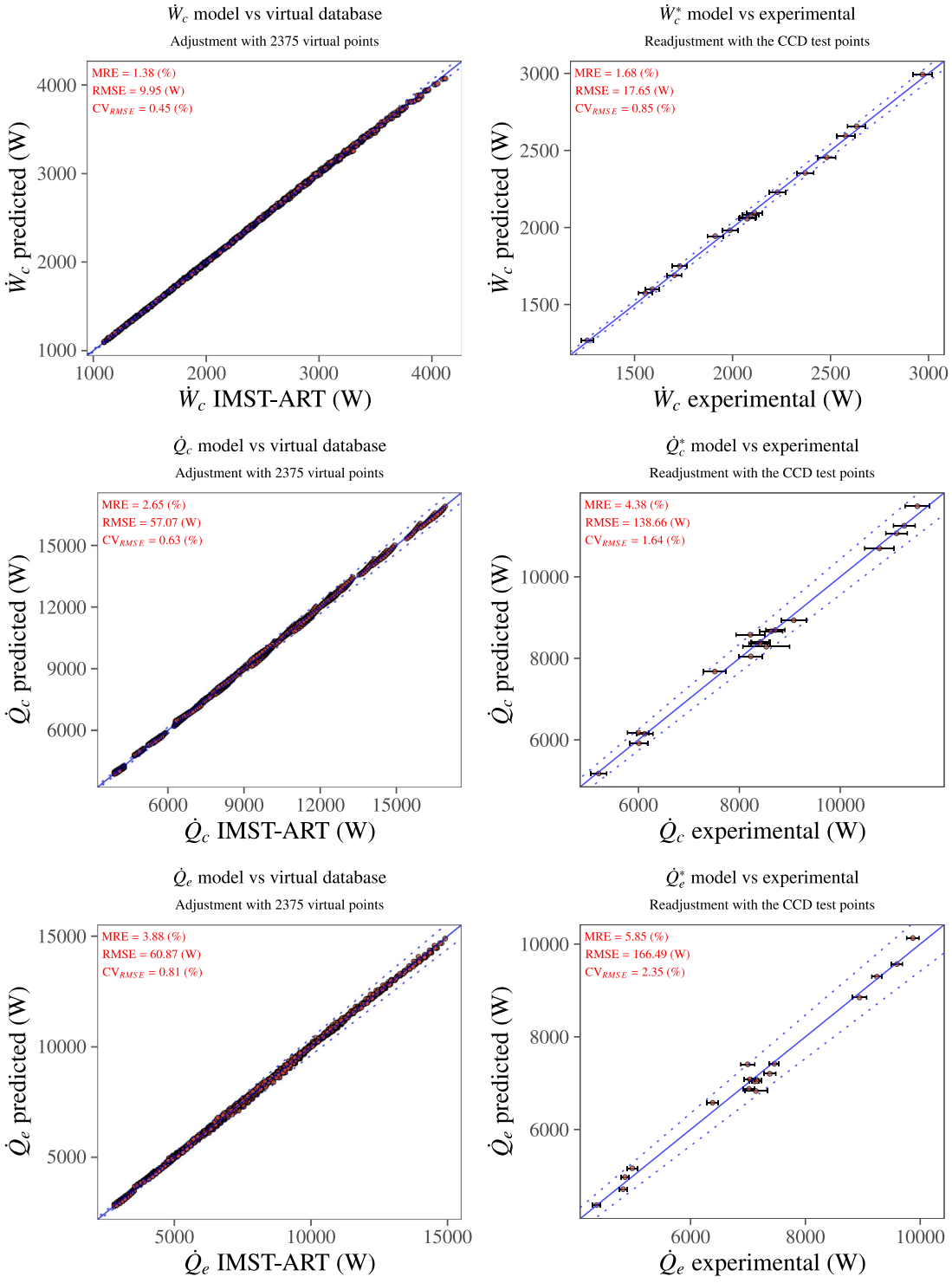

Fig. A.7. DHW Air mode: Empirical model.

Appendix B. Example of compressor energy consumption model in WG mode

See Example 2 which includes an example of how to recompose the model with the summarized data provided in Appendix A for the $\dot{W}_c$ prediction in Winter Ground mode.

Example 2: WG: Final polynomial model for the $\dot{W}_c$ prediction

Polynomial model:

$$\dot{W}_c = f_c \cdot (a_0 + a_1 \cdot T_{co}^2 + a_2 \cdot T_{co} + a_3 \cdot T_{eo}^2 + a_4 \cdot T_{eo} + a_5 \cdot dT_c + a_6 \cdot dT_e + a_7 \cdot f_c + a_8 \cdot 1/f_c + a_9 \cdot T_{co} \cdot T_{eo} + a_{10} \cdot T_{co} \cdot dT_c + a_{11} \cdot T_{eo} \cdot f_c)$$

$$\left.\frac{\partial \dot{W}_c}{\partial f_c}\right|_0 = (a_0 + a_1 T_{co0}^2 + a_2 T_{co0} + a_3 T_{eo0}^2 + a_4 T_{eo0} + a_5 dT_{c0} + a_6 dT_{e0} + a_7 f_{c0} + a_8 1/f_{c0} + a_9 T_{co0} T_{eo0} + a_{10} T_{co0} dT_{c0} + a_{11} T_{eo0} f_{c0}) + f_{c0}(a_7 - a_8 1/f_{c0}^2 + a_{11} T_{eo0}) = 5.186\text{e+}01$$

$$\left.\frac{\partial \dot{W}_c}{\partial T_{eo}}\right|_0 = f_{c0}(a_3(2T_{eo0}) + a_4 + a_9 T_{co0} + a_{11} f_{c0}) = 7.033\text{e+}00$$

$$\left.\frac{\partial \dot{W}_c}{\partial dT_e}\right|_0 = a_6 f_{c0} = 1.587\text{e+}00$$

$$\left.\frac{\partial \dot{W}_c}{\partial T_{co}}\right|_0 = f_{c0}(a_1(2T_{co0}) + a_2 + a_9 T_{eo0} + a_{10} dT_{c0}) = 3.859\text{e+}01$$

$$\left.\frac{\partial \dot{W}_c}{\partial dT_c}\right|_0 = f_{c0}(a_5 + a_{10} T_{co0}) = -1.304\text{e+}01$$

where:

$a_0 = 1.162\text{e+}03$	$a_3 = -3.968\text{e-}03$	$a_6 = 3.174\text{e-}02$	$a_9 = 1.089\text{e-}02$
$a_1 = 7.612\text{e-}03$	$a_4 = -1.214\text{e+}00$	$a_7 = -1.602\text{e-}01$	$a_{10} = -1.029\text{e-}02$
$a_2 = -6.997\text{e+}00$	$a_5 = 3.013\text{e+}00$	$a_8 = 2.991\text{e+}02$	$a_{11} = 1.125\text{e-}03$

CCD center point:

$\dot{W}_{c0} = 1856.612$ (W)	$dT_{e0} = 4.972$ (K)
$f_{c0} = 50$ (Hz)	$T_{co0} = 318.272$ (K)
$T_{eo0} = 273.184$ (K)	$dT_{c0} = 5.078$ (K)

Polynomial model adjusted:

$$\dot{W}_c^* = \dot{W}_c + (k_1 - 1) \cdot \left.\frac{\partial \dot{W}_c}{\partial f_c}\right|_0 \cdot (f_c - f_{c0}) + (k_2 - 1) \cdot \left.\frac{\partial \dot{W}_c}{\partial T_{eo}}\right|_0 \cdot (T_{eo} - T_{eo0}) + (k_3 - 1) \cdot \left.\frac{\partial \dot{W}_c}{\partial dT_e}\right|_0 \cdot (dT_e - dT_{e0}) + (k_4 - 1) \cdot \left.\frac{\partial \dot{W}_c}{\partial T_{co}}\right|_0 \cdot (T_{co} - T_{co0}) + (k_5 - 1) \cdot \left.\frac{\partial \dot{W}_c}{\partial dT_c}\right|_0 \cdot (dT_c - dT_{c0}) + (k_0 - 1) \cdot \dot{W}_{c0}$$

where:

$k_0 = 1.000\text{e+}00$	$k_2 = 1.070\text{e+}00$	$k_4 = 1.046\text{e+}00$
$k_1 = 9.815\text{e-}01$	$k_3 = 1.274\text{e+}00$	$k_5 = 1.163\text{e+}00$

Appendix C. Supplementary data

Supplementary material related to this article can be found online at https://doi.org/10.1016/j.applthermaleng.2024.123724.

References

[1] European Commission, Directive 2012/27/EU on energy efficiency, amending Directives 2009/125/EC and 2010/30/EU and repealing Directives 2004/8/EC and 2006/32/EC, 2012.

[2] European Commission, Com(2016) 51: An EU strategy on heating and cooling, 2016.

[3] European Commission, COM(2022) 230: REPowerEU Plan, 2022.

[4] P. Bayer, D. Saner, S. Bolay, L. Rybach, P. Blum, Greenhouse gas emission savings of ground source heat pump systems in Europe: A review, Renew. Sustain. Energy Rev. 16 (2) (2012) 1256–1267, http://dx.doi.org/10.1016/j.rser.2011.09.027.

[5] S.J. Rees, Advances in Ground-Source Heat Pump Systems, Elsevier Inc., 2016, pp. 1–460, http://dx.doi.org/10.1016/C2014-0-03840-3.

[6] Y. Nam, R. Ooka, Y. Shiba, Development of dual-source hybrid heat pump system using groundwater and air, Energy Build. 42 (6) (2010) 909–916, http://dx.doi.org/10.1016/j.enbuild.2009.12.013.

[7] S. Marinelli, F. Lolli, M.A. Butturi, B. Rimini, R. Gamberini, Environmental performance analysis of a dual-source heat pump system, Energy Build. 223 (2020) 110180, http://dx.doi.org/10.1016/j.enbuild.2020.110180.

[8] C. Fischer, ORNL Heat Pump Model: A Steady-State Computer Design Model of Air-to-Air Heat Pumps, Oak Ridge National Laboratory (ORNL), Oak Ridge, TN (United States), 1983, http://dx.doi.org/10.2172/814817, Fortran-IV computer program.

[9] J. Brown, R. Brignoli, P. Domanski, Y. Yoon, CYCLE_D-HX: NIST Vapor Compression Cycle Model Accounting for Refrigerant Thermodynamic and Transport Properties; Version 2, User's Guide, Technical Note (NIST TN), National Institute of Standards and Technology, Gaithersburg, MD, 2021, http://dx.doi.org/10.6028/NIST.TN.2134.

[10] J.M. Corberán, J. Gonzálvez, P. Montes, R. Blasco, 'Art' a computer code to assist the design of refrigeration and A/C equipment, in: International Refrigeration and Air Conditioning Conference. Paper 570, Purdue University, West Lafayette, Indiana, 2002.

[11] J.J. Allen, J.F. Hamilton, Steady-state reciprocating water chiller models, in: Annual Meeting, Vol. 89, No. 2, Washington DC, ASHRAE Transactions, 1983, pp. 398–407.

[12] S.A. Tabatabaei, J. Treur, E. Waumans, Comparative evaluation of different computational models for air source heat pump based on real word data, in: Energy Procedia, vol. 95, Elsevier Ltd, 2016, pp. 459–466, http://dx.doi.org/10.1016/j.egypro.2016.09.065.

[13] C. Verhelst, F. Logist, J. Van Impe, L. Helsen, Study of the optimal control problem formulation for modulating air-to-water heat pumps connected to a residential floor heating system, Energy Build. 45 (2012) 43–53, http://dx.doi.org/10.1016/j.enbuild.2011.10.015.

[14] H. Cheung, S. Wang, A comparison of the effect of empirical and physical modeling approaches to extrapolation capability of compressor models by uncertainty analysis: A case study with common semi-empirical compressor mass flow rate models, Int. J. Refrig. 86 (2018) 331–343, http://dx.doi.org/10.1016/j.ijrefrig.2017.11.020.

[15] AHRI 540, AHRI 540 - Standard for Performance Rating of Positive Displacement Refrigerant Compressors and Compressor Units, Air-Conditioning, Heating, and Refrigeration Institute (AHRI), 2020.

[16] J. Marchante-Avellaneda, E. Navarro-Peris, Y. Song, Development of map-based models for the performance characterization in a new prototype of Dual Source Heat Pump, Appl. Therm. Eng. 236 (2024) 121743, http://dx.doi.org/10.1016/j.applthermaleng.2023.121743.

[17] European Commission, Geothermal technology for €conomic cooling, 2015, *(H2020-LCE-2014-2, GEOTeCH-656889)*.

[18] J. Marchante Avellaneda, Study of Response Surface Models for the characterization of the performance in Refrigeration Equipments and Heat Pumps (Ph.D. thesis), Universitat Politècnica de València, 2023, http://dx.doi.org/10.4995/Thesis/10251/192653.

[19] R. Core Team, R: A Language and Environment for Statistical Computing, R Foundation for Statistical Computing, Vienna, Austria, 2022, Version 4.1.3.

[20] RStudio Team, RStudio: Integrated Development Environment for R, RStudio, PBC, Boston, MA, 2022.

[21] Thermal Area IUIIE, IMST-ART: A Simulation Tool to Assist the Selection, Design and Optimization of Refrigeration Equipments and Components, IMST-GROUP, Instituto de Ingeniería Energética (Universitat Politècnica de València), Camino de Vera S/N, 46022, Valencia (Spain), 2019, Version 3.9.

[22] S. Klein, EES: Engineering Equation Solver, F-Chart Software, Madison, Wisconsin 53744, USA, 2020, Version 10.833.

[23] G.E. Box, N.R. Draper, Response Surfaces, Mixtures and Ridge Analyses, second ed., John Wiley & Sons, Inc., 2007.

[24] G.E.P. Box, K.B. Wilson, On the experimental attainment of optimum conditions, J. R. Stat. Soc. Ser. B Stat. Methodol. 13 (1) (1951) 1–38.

[25] G.E.P. Box, D.W. Behnken, Some new three level desing for study of quantitative variables, Technometrics 2 (4) (1960) 455–475.

[26] S. Fisher, The Design of Experiments, ninth ed., Hafner Press, New York, 1971.

[27] G. Taguchi, System of Experimental Design: Engineering Methods to Optimize Quality and Minimize, Quality Resources (Kraus), New York, 1987.

[28] N.A. Heckert, J.J. Filliben, C.M. Croarkin, B. Hembree, W.F. Guthrie, P. Tobias, J. Prinz, Handbook 151: NIST/SEMATECH e-Handbook of Statistical Methods, National Institute of Standards and Technology, Gaithersburg, MD, 2002, http://dx.doi.org/10.18434/M32189.

[29] University of York, L16b Orthogonal Array, 2024.

[30] J.M. Corberán, J. Marchante-Avellaneda, S. Bortolin, L. Moro, E. Zanetti, D. Del Col, G. Busato, Deliverable D4.5. Experimental results of prototypes: 1-3, 2017, WP4 Plug&Play Geothermal System Development. GEOTeCH-656889.